

Theory of transverse magnetization in spin-orbit coupled antiferromagnets

Taekoo Oh,^{1,2,3} Sungjoon Park,^{1,2,3} and Bohm-Jung Yang^{1,2,3,*}

¹Department of Physics and Astronomy, Seoul National University, Seoul 08826, Korea

²Center for Correlated Electron Systems, Institute for Basic Science (IBS), Seoul 08826, Korea

³Center for Theoretical Physics (CTP), Seoul National University, Seoul 08826, Korea

(Dated: September 14, 2022)

Some antiferromagnets under a magnetic field develop magnetization perpendicular to the field as well as more conventional ones parallel to the field. So far, the transverse magnetization (TM) has been attributed to either spin canting effect or the presence of cluster magnetic multipolar ordering. However, a general theory of TM based on microscopic understanding is still missing. Here, we construct a general microscopic theory of TM in antiferromagnets with cluster magnetic multipolar ordering by considering classical spin Hamiltonians with spin anisotropy that arises from the spin-orbit coupling. First, from general symmetry analysis, we show that TM can appear only when all crystalline symmetries are broken other than the antiunitary mirror, antiunitary two-fold rotation, and inversion symmetries. Moreover, by analyzing spin Hamiltonians, we show that TM always appears when the degenerate ground state manifold of the spin Hamiltonian is discrete. On the other hand, when the degenerate ground state manifold is continuous, TM generally does not appear except when the magnetic field direction and the spin configuration satisfy specific geometric conditions under single-ion anisotropy. Finally, we show that TM can induce anomalous planar Hall Effect, a unique transport phenomenon that can be used to probe multipolar antiferromagnetic structures. We believe that our theory provides a useful guideline for understanding the anomalous magnetic responses of the antiferromagnets with complex magnetic structures.

Introduction.— Spin-orbit coupled antiferromagnets are a promising playground to study novel correlated topological states and anomalous transport phenomena.^{1,2} The complex spin structures of spin-orbit coupled antiferromagnets can be characterized by their cluster magnetic multipole (CMM) moments reflecting the symmetry of the magnetic ground state.^{3,4} Especially, those with higher-rank CMMs can exhibit anomalous transport phenomena including various types of anomalous Hall effects.^{3–16} The distinct magnetic symmetry of higher-rank CMMs underlies their unconventional physical properties, unexpected in simple spin systems with magnetic dipoles only.

Normally, when a magnetic field \mathbf{B} is applied to an antiferromagnet, the magnetization is developed along the field direction. However, in several antiferromagnets with spin anisotropy including $\text{Gd}_2\text{Ti}_2\text{O}_7$, CsMnBr_3 , and $\text{Eu}_2\text{Ir}_2\text{O}_7$,^{17–22} transverse magnetization (TM) was also observed. More specifically, in $\text{Gd}_2\text{Ti}_2\text{O}_7$ and CsMnBr_3 , TM was observed when \mathbf{B} was along certain directions and was attributed to the spin canting effect. More recently, TM was also observed in $\text{Eu}_2\text{Ir}_2\text{O}_7$. But in this system, the presence of a magnetic octupolar ordering, not the spin canting effect, was proposed as the origin of TM based on phenomenological Landau theory, and the resultant TM was dubbed the orthogonal magnetization (OM).²¹ One common feature of the three systems in which TM was observed is that the antiferromagnetic ground state has higher-rank CMM and the relevant spin Hamiltonian has spin-anisotropy arising from spin-orbit coupling. Thus, to understand the fundamental origin of TM, the relation between the spin anisotropy and the complex magnetic structure with higher-rank CMM should be clarified.

In this Letter, we construct a general microscopic theory of TM. First, through symmetry analysis, we derive the general symmetry condition to have TM. Explicitly, we show that TM emerges only when every crystalline symmetry is broken,

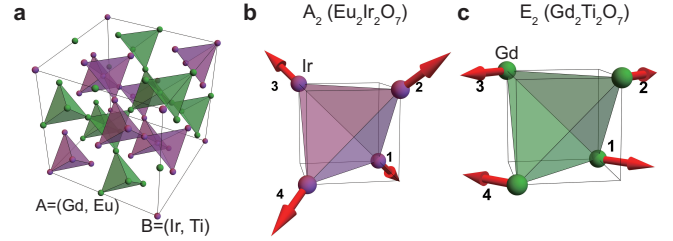


FIG. 1. (a) Structure of the pyrochlore lattice relevant to $\text{Gd}_2\text{Ti}_2\text{O}_7$ and $\text{Eu}_2\text{Ir}_2\text{O}_7$. (b, c) Spin configurations of (b) A_2 -octupole in $\text{Eu}_2\text{Ir}_2\text{O}_7$ and (c) E_2 -dotriacontapole in $\text{Gd}_2\text{Ti}_2\text{O}_7$.

except for twofold antiunitary rotation C_2T , antiunitary mirror σT , and inversion P . Here, C_2 , σ , T indicate two-fold rotation, mirror, and time-reversal symmetries, respectively. Based on the symmetry, we further tabulate the information about whether TM is allowed or not under various field directions for all possible antiferromagnetic structures relevant to Mn_3Ir , CsMnBr_3 , and pyrochlore systems including $\text{Gd}_2\text{Ti}_2\text{O}_7$ and $\text{Eu}_2\text{Ir}_2\text{O}_7$.

We also examine the microscopic origin of TM by studying the classical spin Hamiltonian on the pyrochlore lattice with spin anisotropy represented by single-ion anisotropy (SIA), Dzyaloshinskii-Moriya interaction (DMI), and dipolar interaction (DI). Depending on the nature of spin anisotropy, the antiferromagnetic ground state has distinct CMMs, and the degenerate ground state manifold (DGSM) is either discrete or continuous under spin rotation. We find that when DGSM is discrete, TM always appears unless forbidden by symmetry. On the other hand, when DGSM is continuous, TM is generally not allowed. However, when DGSM is constrained in easy planes by SIA, TM can appear when the magnetic field direction and spin configuration satisfy certain geometric conditions. As a result of TM, we show that TM induces a unique

transport phenomenon called anomalous planar Hall Effect (APHE).²³ Although we mainly focus on the pyrochlore lattice, our theory can be readily generalized to any antiferromagnets on any lattice system.

Global symmetry constraints.— Let us first consider the symmetry constraint on the TM (\mathbf{M}_\perp) under \mathbf{B} . First, we note that any n -fold rotation symmetry C_n ($n = 2, 3, 4, 6$) along the direction of \mathbf{B} prohibits nonzero TM because \mathbf{M}_\perp is canceled by its rotated counterparts $\sum_{i=1}^{n-1} C_n^i \mathbf{M}_\perp$. Similarly, a mirror symmetry σ with the normal direction parallel to \mathbf{B} also forbids the TM. The only unitary symmetry compatible with nonzero TM is spatial inversion P .

In the case of antiunitary symmetries, there are two symmetries compatible with $\mathbf{M}_\perp \neq 0$. One is C_2T symmetry whose rotation axis is perpendicular to \mathbf{B} . In this case, \mathbf{M}_\perp perpendicular to both \mathbf{B} and the C_2 rotation axis can be nonzero. The other is σT symmetry whose mirror plane is parallel to \mathbf{B} . Then, \mathbf{M}_\perp can appear parallel to the mirror plane. As the combination of C_2T and σT is just P , \mathbf{M}_\perp can emerge even when both symmetries exist simultaneously. In summary, every symmetry except for C_2T , σT , and P must be broken to have $\mathbf{M}_\perp \neq 0$.

Using this symmetry condition, one can judge whether \mathbf{M}_\perp is forbidden or not in any antiferromagnetic (AFM) system under various field directions. In the case of AFM orders in the pyrochlore lattice with a tetrahedral magnetic unit cell shown in Fig. 1, the magnetic structures can be classified by using group theory, and the resulting irreducible representations (IRREPs) can be described in terms of CMMs^{3,4} including A_2 -octupole (A_2), T_1 -octupoles (T_{1x}, T_{1y}, T_{1z}), T_2 -octupoles (T_{2x}, T_{2y}, T_{2z}), and E -dotriacontapoles (E_1, E_2).^{3,4,21,24–28} In the case of the A_2 -octupole shown in Fig. 1, for example, its magnetic point group is $-4'3m'$ composed of an identity I , 3 two-fold rotations C_2 , 8 threefold rotations C'_3 , 6 antiunitary mirrors σT , and 6 four-fold antiunitary inversion S_4T . For $\mathbf{B} \parallel [001]$, every symmetry except I , C_{2z} , and two σT s is broken. Because there is C_{2z} , $\mathbf{M}_\perp = 0$. On the other hand, when $\mathbf{B} \parallel [110]$, only I and a σT remain, thus \mathbf{M}_\perp can be nonzero. We extend this analysis to D_{3h} point group relevant to CsMnBr_3 ¹⁷ and to O_h point group relevant to Mn_3Ir ,^{3,16,29–32} as summarized in Appendix.

The analysis of the magnetic point group symmetry under \mathbf{B} can also determine the direction of \mathbf{M}_\perp and its general \mathbf{B} dependence. For instance, let us consider an AFM ordering with the magnetic point group P , which is described by the Hamiltonian $H(\{\mathbf{S}_a\})$ where a is a sublattice index. When \mathbf{B} is applied, the symmetries in P will be mostly broken but they still strongly constrain the spin canting directions. More explicitly, for an element $O_p \in P$, we have

$$U(O_p)H(\{\mathbf{S}_a\}, \mathbf{B})U(O_p)^{-1} = H(\{\mathbf{S}_a\}, \mathbf{B}_p), \quad (1)$$

where $\mathbf{B}_p = O_p \mathbf{B}$ and $U(O_p)$ is the matrix representation of O_p . Namely, O_p effectively changes the direction of \mathbf{B} while keeping the spin structure. For example, let us consider the A_2 -octupole under $\mathbf{B} \parallel [110]$ again. Among the symmetries in P , $P_1 = \{I, \sigma_{[1\bar{1}0]}T\}$ indicates the symmetry that leaves \mathbf{B} invariant. Here I denotes the identity and $\sigma_{[1\bar{1}0]}$ is

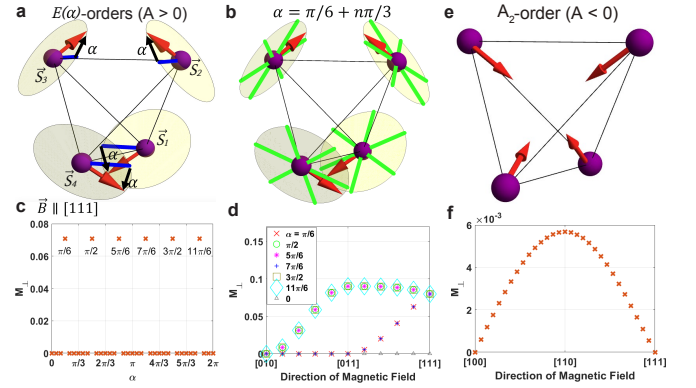


FIG. 2. (a) $\hat{E}(\alpha)$ -order when $A > 0$. The spins (red arrows) are lying on their easy planes (yellow planes). (b) Green lines denote the spin directions of $E(\pi/6 + n\pi/3)$ -orders ($n = 0, \dots, 5$). (c) \mathbf{M}_\perp for $\hat{E}(\alpha)$ -order as a function of α when $\mathbf{B} \parallel [111]$. $\mathbf{M}_\perp \neq 0$ only at $\alpha = \pi/6 + n\pi/3$. (d) \mathbf{M}_\perp for $\hat{E}(\alpha)$ -order with various α computed by changing \mathbf{B} from $[010]$ to $[011]$, and to $[111]$. (e) A_2 -order when $A < 0$. (f) \mathbf{M}_\perp for A_2 -order computed by changing \mathbf{B} from $[100]$ to $[110]$, and to $[111]$. In (c,d,f), we choose $|A|/J = B/J = 1$.

the mirror symmetry whose normal direction is along $[1\bar{1}0]$. On the other hand, $P_2 = \{C_{2z}, \sigma_{[110]}T\}$ denotes the symmetries which invert the direction of \mathbf{B} . Here $\sigma_{[110]}$ is the mirror symmetry whose normal direction is along $[110]$. Applying P_1 and P_2 symmetries to the constraint equation in Eq. (1), we obtain $\mathbf{M}_\perp \propto [bB^2 + O(B^4)] \hat{z}$ with a constant b . A similar analysis can also be applied to other CMMs. In the case of E_2 -dotriacontapole under $\mathbf{B} \parallel [111]$, we find that $P_1 = \{I\}$ leaves \mathbf{B} invariant while $P_2 = \{\sigma_{1\bar{1}0}\}$, inverts the \mathbf{B} direction, which gives $\mathbf{M}_\perp = (bB^2 + \dots)\hat{e}_{1\bar{1}0} + (dB + fB^3 + \dots)\hat{e}_{11\bar{2}}$ where b, d, f are constants. Detailed \mathbf{B} dependence of TM is determined by microscopic spin interactions as discussed below. The cases of E_1 and T_{2y} CMMs under $\mathbf{B} \parallel [111]$ are further analyzed in Appendix.

Microscopic Hamiltonian.— The classical Heisenberg antiferromagnet on the pyrochlore lattice has macroscopically degenerate ground states.^{33,34} Under a magnetic field \mathbf{B} , the Hamiltonian can be written as

$$\begin{aligned} H_0 = H_J + H_B &= J \sum_{\langle ab \rangle} \mathbf{S}_a \cdot \mathbf{S}_b - \sum_a \mathbf{B} \cdot \mathbf{S}_a, \\ &= 8JN_c \mathbf{M}^2 - 4N_c \mathbf{B} \cdot \mathbf{M} - \frac{JN_c}{2} \sum_{a=1}^4 \mathbf{S}_a^2, \end{aligned} \quad (2)$$

where H_J with $J > 0$ indicates the isotropic antiferromagnetic exchange interaction between nearest-neighboring spins, and H_B is the Zeeman coupling. N_c is the number of tetrahedral unit cells, $\mathbf{M} = \frac{1}{4} \sum_{a=1}^4 \mathbf{S}_a$ is the average magnetization of the four spins in a tetrahedron. From $\mathbf{S}_a^2 = 1$, we obtain $H_0 = 8JN_c(\mathbf{M} - \frac{\mathbf{B}}{4J})^2$. Then, the minimum energy condition gives $\mathbf{M} = \frac{\mathbf{B}}{4J}$. Namely, TM does not appear when spin anisotropy is absent.

Single-ion anisotropy (SIA).— Let us consider $H_1 \equiv H_0 + H_{SIA}$ that includes the SIA, $H_{SIA} = A \sum_a (\mathbf{S}_a \cdot \mathbf{n}_a)^2$. When $A > 0$, H_{SIA} forces \mathbf{S}_a to lie on its easy plane on which

$\mathbf{S}_a \cdot \mathbf{n}_a = 0$ is satisfied [see Fig. 2a]. The energy minimum condition of H_1 is

$$\mathbf{M} = \frac{\mathbf{B}}{4J}, \quad \mathbf{S}_a \cdot \mathbf{n}_a = 0 \quad (a = 1, 2, 3, 4). \quad (3)$$

When $\mathbf{B} = 0$, the ground state is antiferromagnetic with either E -dotriacontapole or T_2 -octupole, in which all spins are lying on their easy-planes. As the E -dotriacontapole belongs to a two-dimensional (2D) IRREP, it is composed of two basis states called the \hat{E}_1 and \hat{E}_2 -orders. Similarly, the T_2 -octupole belonging to a three-dimensional (3D) IRREP is composed of three basis states, called the \hat{T}_{2x} , \hat{T}_{2y} , and \hat{T}_{2z} -orders [see Appendix].

More specifically, in the \hat{E}_1 -order, the four spins $\mathbf{S}_{a=1,2,3,4}$ in a unit cell are aligned along the directions $\hat{x}_1 = [\bar{1}\bar{1}0]$, $\hat{x}_2 = [110]$, $\hat{x}_3 = [\bar{1}\bar{1}0]$, $\hat{x}_4 = [110]$, respectively, while for the \hat{E}_2 -order, the spins are along $\hat{y}_1 = [11\bar{2}]$, $\hat{y}_2 = [\bar{1}\bar{1}2]$, $\hat{y}_3 = [11\bar{2}]$, $\hat{y}_4 = [\bar{1}\bar{1}2]$, respectively. Then a general E -dotriacontapole order can be represented by $\hat{E}(\alpha) = \hat{E}_1 \sin \alpha + \hat{E}_2 \cos \alpha$, which spans a continuous DGSM parametrized by $0 \leq \alpha \leq 2\pi$ [see Fig. 2a]. As α varies, the spins continuously rotate on their easy planes. Similar to (\hat{E}_1, \hat{E}_2) -orders, $(\hat{E}(\alpha = \pi/6), \hat{T}_{2x})$ -orders, $(\hat{E}(\alpha = 5\pi/6), \hat{T}_{2y})$ -orders, and $(\hat{E}(\alpha = \pi/2), \hat{T}_{2z})$ -orders form pairs of basis states which span continuous DGSM where spins are lying on their easy planes.

When $\mathbf{B} \neq 0$, the energy minimum condition in Eq. (3) is satisfied in most cases, thus TM vanishes. But there are a few exceptional cases with nonzero TM. For example, for a given $\hat{E}(\alpha)$ order at $\mathbf{B} = 0$, the spin configuration at small \mathbf{B} can be parametrized as

$$\mathbf{S}_a = \cos \theta_a [\cos(\alpha + \phi_a) \hat{x}_a + \sin(\alpha + \phi_a) \hat{y}_a] - \sin \theta_a \hat{z}_a, \quad (4)$$

where ϕ_a (θ_a) indicates the rotation within (away from) the easy-plane of \mathbf{S}_a due to $\mathbf{B} \neq 0$. At small \mathbf{B} , we expand \mathbf{S}_a up to the first order of (θ_a, ϕ_a) and put it in Eq. (3), which gives $\mathbf{S}_a \cdot \mathbf{n}_a = -\theta_a = 0$, $M_x = \frac{1}{4\sqrt{6}} [(\cos \alpha - \sqrt{3} \sin \alpha)(\phi_1 + \phi_2 - \phi_3 - \phi_4)]$, $M_y = \frac{1}{4\sqrt{6}} [(\cos \alpha + \sqrt{3} \sin \alpha)(\phi_1 - \phi_2 + \phi_3 - \phi_4)]$, $M_z = \frac{-1}{2\sqrt{6}} [\cos \alpha (\phi_1 - \phi_2 - \phi_3 + \phi_4)]$. Note that when $\tan \alpha = 1/\sqrt{3}$, $M_x = 0$. Then, $M_x = B_x/(4J)$ in Eq. (3) cannot be satisfied if $B_x \neq 0$. Similar situations occur when $\tan \alpha = -1/\sqrt{3}$ and $B_y \neq 0$, or $\cos \alpha = 0$ and $B_z \neq 0$.

Interestingly, these are exactly the conditions to have nonzero TM [see Fig. 2b]. For instance, for the $\hat{E}(\alpha = \pi/6, 7\pi/6)$ order with $\tan \alpha = 1/\sqrt{3}$, when $\mathbf{B} \parallel [100]$, the projection of \mathbf{B} onto the easy plane of each spin is parallel to the corresponding spin direction, thus \mathbf{B} cannot rotate each spin within its easy plane. Instead, \mathbf{B} forces the spins to move away from their easy planes, which makes the energy minimum condition in Eq. (3) to be violated and induces nonzero TM. Similar situations happen for $\hat{E}(5\pi/6, 11\pi/6)$ order with $B_y \neq 0$, and $\hat{E}(\pi/2, 3\pi/2)$ order with $B_z \neq 0$.

The spin configuration with nonzero TM can be obtained by the stationary condition $\partial H_1 / \partial \theta_a = \partial H_1 / \partial \phi_a = 0$. For instance, for $\hat{E}(\pi/2)$ order under $\mathbf{B} \parallel [111]$ described in Fig. 2b,

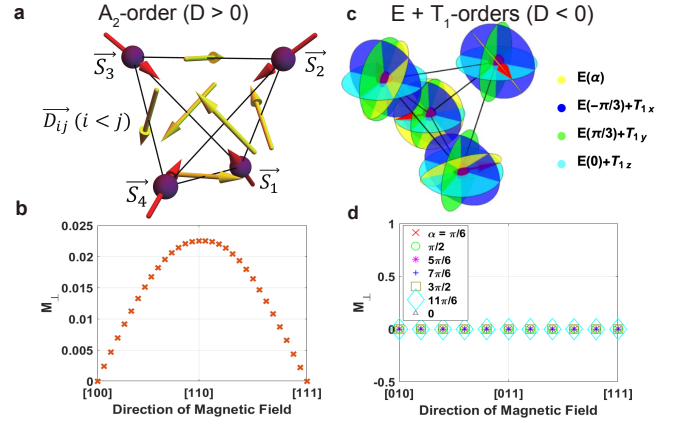


FIG. 3. (a) A_2 -order when $D > 0$, where all spins (red arrows) are perpendicular to the surrounding DM vectors (yellow arrows). (b) M_{\perp} for A_2 -order computed by changing \mathbf{B} from [100] to [110] and to [111]. (c) Schematic description of continuous DGSM when $D < 0$. There are four distinct planes; yellow planes are for $E(\alpha)$ -order, blue planes are for $E(-\pi/3) + T_{1x}$ -order, green planes are for $E(\pi/3) + T_{1y}$ -order, and cyan planes are for $E(0) + T_{1z}$ -order. (d) M_{\perp} for $\hat{E}(\alpha)$ -order with various α computed by changing \mathbf{B} from [010] to [011] and to [111]. In (b,d), we assume $|D|/J = B/J = 1$.

the stationary condition gives $\theta_1 = \theta_4 = -\theta_2 = -\theta_3 = \frac{B}{6A+4J}$, $\phi_1 = \phi_4 = 0$, $\phi_2 = -\phi_3 = -\frac{B}{\sqrt{6}J}$, from which we obtain $M_{\perp} = \frac{\sqrt{2}}{4(2+3A/J)} (\frac{A}{J})(\frac{B}{J}) \hat{e}_{11\bar{2}}$. We note that as $\theta_{1,2,3,4}$ are nonzero, all spins move away from their easy planes. In Fig. 2c, we compute M_{\perp} for $\hat{E}(\alpha)$ order under $\mathbf{B} \parallel [111]$ varying α . In Fig. 2d, we plot M_{\perp} for various $\hat{E}(\alpha)$ -orders by continuously rotating \mathbf{B} from [010] to [011], and then to [111] in sequence. M_{\perp} becomes nonzero only when the special conditions between \mathbf{B} and α described above are satisfied. [See Appendix for further discussions.]

When $A < 0$, on the other hand, each spin \mathbf{S}_a aligns along its easy axis direction \mathbf{n}_a , leading to the all-in all-out ground state with an A_2 -octupolar moment shown in Fig. 2e. Two degenerate ground states, all-in or all-out state, related by time-reversal symmetry form a discrete manifold in which the states are separated by an energy barrier, contrary to the $A > 0$ case. In this situation, we find that TM can generally appear unless it is forbidden by symmetry. We compute the TM by changing \mathbf{B} from [010] to [101], and then to [111] continuously, and represent the result in Fig. 2f. Note that considering symmetry, TM vanishes for $\mathbf{B} \parallel [001]$ and [111]. For other directions, TM is nonzero and exhibits $|M_{\perp}| \propto (A/J)(B/J)^2$ consistent with magnetic space group analysis. All these results are further confirmed by numerically solving H_1 using mean-field theory [see Appendix].

Dzyaloshinskii-Moriya interaction (DMI).— Next, we consider $H_2 \equiv H_0 + H_{DMI}$ that includes the DMI, $H_{DMI} = D \sum_{\langle ab \rangle} \hat{\mathbf{D}}_{ab} \cdot (\mathbf{S}_a \times \mathbf{S}_b)$. Generally, DMI forces two spins \mathbf{S}_a and \mathbf{S}_b to lie in their planes perpendicular to the DM vector $\hat{\mathbf{D}}_{ab}$ so that $\mathbf{S}_a \times \mathbf{S}_b$ is anti-parallel (parallel) to $\hat{\mathbf{D}}_{ab}$ when $D > 0$ ($D < 0$).

Let us first consider $D > 0$ case.²⁷ In the pyrochlore lattice,

DMI forces each spin to be perpendicular to its six neighboring DM vectors, and the intersection between the planes normal to those DM vectors is uniquely determined, which leads to the A_2 -order as shown in Fig. 3a. As in the case of SIA with $A < 0$, since DGSM is discrete, TM can generally arise unless prohibited by symmetry. For example, in Fig. 3b, we compute the TM by changing \mathbf{B} from $[100]$ to $[110]$, and then to $[111]$. When $\mathbf{B} \parallel [100]$ and $[111]$, TM vanishes because of rotation symmetries. Otherwise, TM is nonzero. From the stationary condition of H_2 , we obtain $|\mathbf{M}_\perp| \propto (\frac{D}{J})(\frac{B^2}{J^2})$. [See Appendix for more details.]

On the other hand, when $D < 0$, the relative angle between neighboring spins should be inverted compared to $D > 0$ case to minimize the energy. To find the ground state for $D < 0$, we rewrite H_2 by adding some constants as

$$H_2 = -12D \left(\sum_a \mathbf{S}_a \cdot \hat{v}_a / 4 \right)^2 - 8D \sum_{r=1}^3 \left[\left(\sum_a \mathbf{S}_a \cdot \mathbf{T}_a^r / 4 \right)^2 \right] + 8(J - D/2) \left(\mathbf{M} - \frac{\mathbf{B}}{4(J - D/2)} \right)^2, \quad (5)$$

where \hat{v}_a is the unit vector along the local z -axis of \mathbf{S}_a , and \mathbf{T}_a^r ($r = 1, 2, 3$) indicates the spin direction relevant to T_2 octupolar ordering. The explicit forms of \hat{v}_a and \mathbf{T}_a^r are given in Appendix. Since $D < 0$, all the coefficients of squared terms in H_2 are positive, thus H_2 can be minimized when the following seven equations are satisfied,

$$\mathbf{M} = \frac{\mathbf{B}}{4J - 2D}, \quad \sum_{a=1}^4 \mathbf{S}_a \cdot \hat{v}_a = 0, \quad \sum_{a=1}^4 \mathbf{S}_a \cdot \mathbf{T}_a^r = 0. \quad (6)$$

When $\mathbf{B} = 0$, one can show that (\hat{E}_1, \hat{E}_2) -orders span the continuous DGSM as in the case of SIA with $A > 0$. Similarly, $(\hat{E}(\alpha = 0), \hat{T}_{1z})$ -orders, $(\hat{E}(\alpha = \pi/3), \hat{T}_{1y})$ -orders, and $(\hat{E}(\alpha = -\pi/3), \hat{T}_{1x})$ -orders form pairs of basis states which span continuous DGSM where spins are lying on the xy , zx , and yz planes, respectively. [See Fig. 3c.]

Since DGSM is continuous, one can generally expect TM to be vanishing. To check the possible exceptional situations as in the SIA case with $A > 0$, let us consider $\hat{E}(\alpha)$ order at $\mathbf{B} = 0$ and examine the spin configuration at small \mathbf{B} by introducing angular variation (θ_a, ϕ_a) as in Eq. (4). Plugging the parametrized form of spins in Eq. (4) into Eq. (6), we obtain, up to the linear order in $B = |\mathbf{B}|$, $\theta_a = -3\hat{z}_a \cdot \frac{\mathbf{B}}{4(J - D/2)}$, $\phi_a = q \frac{B}{4(J - D/2)}$ where q is an arbitrary constant. Contrary to the case of SIA with $A > 0$ in which $\theta_a = 0$ is always required to minimize the SIA term irrespective of \mathbf{B} , in the DMI case with $D < 0$, both θ_a and ϕ_a can continuously vary under \mathbf{B} while the energy minimum condition is satisfied. As spins can rotate continuously in three-dimensional space under \mathbf{B} while satisfying Eq. (6), TM does not appear. This is generally true for arbitrary $E(\alpha)$ under arbitrary \mathbf{B} , as shown in Fig. 3d. The same results can be obtained from the stationary conditions $\partial H_2 / \partial \theta_a = \partial H_2 / \partial \phi_a = 0$. All these results can be further confirmed by numerical mean-field calculation of H_2 [see Appendix]. Also, other $\hat{E} + \hat{T}_1$ -type ground states

with continuous DGSM exhibit similar behaviors as discussed in Appendix.

Anomalous Planar Hall Effect (APHE).— In metallic antiferromagnets with CMMs, TM can induce APHE,²³ i.e. simultaneous appearance of anomalous Hall effect (AHE) and planar Hall effect (PHE).^{35–37} Such a thing is possible because an applied in-plane \mathbf{B} can generate both in-plane $\mathbf{M}_{\perp, in}$ and out-of-plane $\mathbf{M}_{\perp, out}$ TM, which give PHE and AHE, respectively. [See Fig. 4a.]

Motivated by the recent experimental observation of AHE and PHE in pyrochlore iridates,^{22,25} we examine APHE in this system with A_2 -order. Assuming $\hat{x} \parallel [110]$, $\hat{y} \parallel [11\bar{2}]$, and $\hat{z} \parallel [111]$, we apply an electric field $\mathbf{E} \parallel \hat{x}$, and rotate \mathbf{B} within $\hat{x}\hat{y}$ -plane. Considering the symmetry of pyrochlore lattice, we find $M_{\perp, out} = (a_0 + a_1 \cos 3\theta + b_1 \sin 3\theta)\hat{z}$, $M_{\perp, in} = (c_1 \cos 3\theta)\hat{p}$ where a_0, a_1, b_1 , and c_1 are constants, and $\hat{p} = (-\sin \theta, \cos \theta, 0)$ is the in-plane unit vector perpendicular to \mathbf{B} . [See Fig. 4a.] Using the phenomenological model for anomalous Hall conductivity (AHC) and planar Hall conductivity (PHC)^{38,39} given by $\sigma_{xy}^{AHE} = \sigma_0 M_{\perp, out}$, $\sigma_{xy}^{PHE} = \sigma_1 B_x B_y + \sigma_2 (B_x M_{\perp, y} + B_y M_{\perp, x}) + \sigma_3 M_{\perp, x} M_{\perp, y}$, we obtain

$$\begin{aligned} \sigma_{xy}^{AHE} &\propto \beta_0 + \beta_1 \cos 3\theta + \beta_2 \sin 3\theta, \\ \sigma_{xy}^{PHE} &\propto \gamma_1 \cos \theta + \gamma_2 \cos 5\theta \\ &\quad + \delta_1 \sin 2\theta + \delta_2 \sin 4\theta + \delta_3 \sin 8\theta, \end{aligned} \quad (7)$$

where $\beta_{0,1,2}$, $\gamma_{1,2}$, and $\delta_{1,2,3}$ are constants. We note that γ_1, γ_2 terms come from σ_2 term in σ_{xy}^{PHE} while $\delta_1, \delta_2, \delta_3$ come from σ_3 term in σ_{xy}^{PHE} .

To confirm the prediction of the above phenomenological theory, we perform self-consistent mean-field calculations of the Hubbard model describing pyrochlore iridates with A_2 -order,^{24,40} and numerically compute the AHC⁴¹ and PHC.³⁵ [See Appendix for details.] For AHC, we consider only the intrinsic Berry curvature contribution while for PHC, we assume constant relaxation time. The resulting AHC (PHC) is plotted using black dots in Fig. 4b (Fig. 4c) which can be fitted by $\sigma_{xy}^{AHE} \propto \beta_0 + \beta_2 \sin 3\theta$ and $\sigma_{xy}^{PHE} \propto \gamma_1 \cos \theta + \delta_1 \sin 2\theta$, respectively, consistent with Eq. (7). We note that experimental data can contain additional terms due to the presence of rare-earth ions and strain, etc..²² As APHE can probe multipolar AFM structures through its relation with TM, it can be further applied to the systems where conventional methods like neutron scattering do not work.^{18–20}

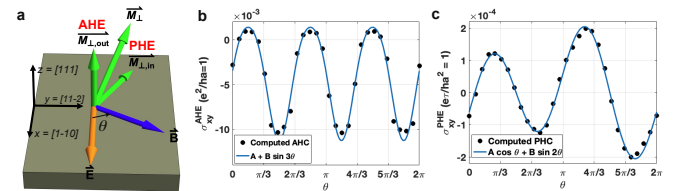


FIG. 4. (a) Schematic description of TM and APHE. (b) The computed AHC (black dots) and its fitting (blue line) by $\beta_0 + \beta_2 \sin 3\theta$. (c) The computed PHC (black dots) and its fitting (blue line) by $\gamma_1 \cos \theta + \delta_1 \sin 2\theta$.

Discussion.— To conclude, we construct a general microscopic theory of TM and identify the symmetry condition to have nonzero TM. When DGSM is discrete, TM is generally allowed unless forbidden by symmetry. On the other hand, when DGSM is continuous, TM generally vanishes except the SIA case with $A > 0$. We have also analyzed the cases with dipolar interactions and obtained nonzero TM due to the discrete DGSM [see Appendix].

Our theory can successfully explain the experimental data for CsMnBr_3 , $\text{Gd}_2\text{Ti}_2\text{O}_7$, $\text{Eu}_2\text{Ir}_2\text{O}_7$ as shown in Appendix. Especially, in the case of $\text{Eu}_2\text{Ir}_2\text{O}_7$, the TM induced by spin canting shows the same behaviors as the OM from phenomenological Landau theory. Thus we think that the spin canting contribution to OM cannot be ruled out to explain the measured data.

ACKNOWLEDGMENT

T.O., S.P., and B.J.Y. were supported by the Institute for Basic Science in Korea (Grant No. IBS-R009-D1), Samsung Science and Technology Foundation under Project Number SSTF-BA2002-06, and the National Research Foundation of Korea (NRF) grant funded by the Korea government (MSIT) (No. 2021R1A2C4002773, and No. NRF-2021R1A5A1032996).

APPENDICES TO "THEORY OF TRANSVERSE MAGNETIZATION IN SPIN-ORBIT COUPLED ANTIFERROMAGNETS"

CONTENTS

A. The symmetry condition for TM	6
B. Cluster Magnetic Multipoles in crystals	7
C. The numerical computations of \mathbf{M}_\perp	11
D. Hubbard model for pyrochlore oxides	11
E. Details in microscopic origin of TM	12
1. Without anisotropy	12
2. Single-ion anisotropy ($A > 0$)	13
3. Single-ion anisotropy ($A < 0$)	15
4. Dzyaloshinskii-Moriya interaction ($D > 0$)	16
5. Dzyaloshinskii-Moriya Interaction ($D < 0$)	17
6. Dipolar interaction	19
F. Application to experiments	20
1. CsMnBr ₃	20
2. Gd ₂ Ti ₂ O ₇	21
3. Eu ₂ Ir ₂ O ₇	21
G. The phenomenological model for anomalous and planar Hall Effect	21
References	22

Appendix A: The symmetry condition for TM

Let us consider the A_2 -order on the pyrochlore lattice under $\mathbf{B} \parallel [110]$. Among the magnetic point group symmetries, $P_1 = \{I, \sigma_{[1\bar{1}0]}T\}$ indicates the symmetry that leaves \mathbf{B} invariant. Here I denotes the identity and $\sigma_{[1\bar{1}0]}$ is the mirror symmetry whose normal direction is along $[1\bar{1}0]$. On the other hand, $P_2 = \{C_{2z}, \sigma_{[110]}T\}$ denotes the symmetries which invert the direction of \mathbf{B} . Here $\sigma_{[110]}$ is the mirror symmetry whose normal direction is along $[110]$. P_1 and P_2 symmetries give the following relations between $\Delta\mathbf{S}_i(\mathbf{B})$:

$$\begin{aligned}
 \Delta\mathbf{S}_{1,\bar{1}0}(\mathbf{B}) &= \Delta\mathbf{S}_{4,\bar{1}0}(\mathbf{B}) = 0, \\
 \Delta\mathbf{S}_{1,z}(\mathbf{B}) &= \Delta\mathbf{S}_{4,z}(-\mathbf{B}), \\
 \Delta\mathbf{S}_{2,\bar{1}0}(\mathbf{B}) &= -\Delta\mathbf{S}_{3,\bar{1}0}(\mathbf{B}) \\
 &= \Delta\mathbf{S}_{2,\bar{1}0}(-\mathbf{B}) = -\Delta\mathbf{S}_{3,\bar{1}0}(-\mathbf{B}), \\
 \Delta\mathbf{S}_{2,z}(\mathbf{B}) &= \Delta\mathbf{S}_{3,z}(\mathbf{B}) \\
 &= \Delta\mathbf{S}_{2,z}(-\mathbf{B}) = \Delta\mathbf{S}_{3,z}(-\mathbf{B}).
 \end{aligned} \tag{A1}$$

Accordingly, the transverse spin change takes the following form

$$\begin{aligned}
 \Delta\mathbf{S}_{1\perp} &= (a_1B + b_1B^2 + c_1B^3 + \dots)\hat{z}, \\
 \Delta\mathbf{S}_{2\perp} &= (b_2B^2 + \dots)\hat{z} + (b_3B^2 + \dots)\hat{e}_{1\bar{1}0}, \\
 \Delta\mathbf{S}_{3\perp} &= (b_2B^2 + \dots)\hat{z} - (b_3B^2 + \dots)\hat{e}_{1\bar{1}0}, \\
 \Delta\mathbf{S}_{4\perp} &= (-a_1B + b_1B^2 - c_1B^3 + \dots)\hat{z},
 \end{aligned} \tag{A2}$$

where a_1, b_1, b_2, b_3 , and c_1 are constants, and $\hat{e}_{1\bar{1}0} = (\hat{x} - \hat{y})/\sqrt{2}$. Note that as the initial directions of \mathbf{S}_2 and \mathbf{S}_3 are perpendicular to \mathbf{B} , their transverse components only have even powers of \mathbf{B} . Hence, we finally obtain the spin TM as

$$\mathbf{M}_\perp \propto [bB^2 + O(B^4)]\hat{z}. \tag{A3}$$

A similar analysis can be applied to any CMM. In the case of E_2 -dotriacontapole under $\mathbf{B} \parallel [111]$, we find that $P_1 = \{I\}$ leaves \mathbf{B} invariant while $P_2 = \{\sigma_{1\bar{1}0}\}$, inverts the \mathbf{B} direction. The constraints by P_1 and P_2 are

$$\begin{aligned}
 \Delta\mathbf{S}_{1/4,1\bar{1}0}(\mathbf{B}) &= \Delta\mathbf{S}_{1/4,1\bar{1}0}(-\mathbf{B}), \\
 \Delta\mathbf{S}_{1/4,11\bar{2}}(\mathbf{B}) &= -\Delta\mathbf{S}_{1/4,11\bar{2}}(-\mathbf{B}), \\
 \Delta\mathbf{S}_{2,1\bar{1}0}(\mathbf{B}) &= \Delta\mathbf{S}_{3,1\bar{1}0}(-\mathbf{B}), \\
 \Delta\mathbf{S}_{2,11\bar{2}}(\mathbf{B}) &= -\Delta\mathbf{S}_{3,11\bar{2}}(-\mathbf{B}),
 \end{aligned} \tag{A4}$$

which give

$$\begin{aligned}
 \Delta\mathbf{S}_{1,\perp} &= (b_1B^2 + \dots)\hat{e}_{1\bar{1}0} + (d_1B + f_1B^3 + \dots)\hat{e}_{11\bar{2}}, \\
 \Delta\mathbf{S}_{2,\perp} &= (a_2B + b_2B^2 + c_2B^3)\hat{e}_{1\bar{1}0} \\
 &\quad + (d_2B + e_2B^2 + f_2B^3)\hat{e}_{11\bar{2}}, \\
 \Delta\mathbf{S}_{3,\perp} &= (-a_2B + b_2B^2 - c_2B^3)\hat{e}_{1\bar{1}0} \\
 &\quad + (d_2B - e_2B^2 + f_2B^3)\hat{e}_{11\bar{2}}, \\
 \Delta\mathbf{S}_{4,\perp} &= (b_4B^2 + \dots)\hat{e}_{1\bar{1}0} + (d_4B + f_4B^3 + \dots)\hat{e}_{11\bar{2}}.
 \end{aligned} \tag{A5}$$

Hence, the spin TM is

$$\mathbf{M}_\perp = (bB^2 + \dots)\hat{e}_{1\bar{1}0} + (dB + fB^3 + \dots)\hat{e}_{11\bar{2}}. \tag{A6}$$

This shows that $\mathbf{M}_\perp \parallel [1\bar{1}0]$ is even in \mathbf{B} while $\mathbf{M}_\perp \parallel [11\bar{2}]$ is odd in \mathbf{B} . In SI, we have also considered E_1 and T_{2y} CMMs under $\mathbf{B} \parallel [111]$. Here, we explain the other cases, E_1 under $\mathbf{B} \parallel [111]$ and T_{2y} under $\mathbf{B} \parallel [111]$. Let G_M is the magnetic point group under the magnetic order. Then, please note that P_1 is the set of G_M elements which keeps \mathbf{B} direction, while P_2 is the set of G_M elements which reverses \mathbf{B} direction.

Next, let us think of E_1 under $\mathbf{B} \parallel [111]$. Then, $P_1 = \{I, \sigma_{[1\bar{1}0]}T\}$, $P_2 = \phi$. The condition is given by

$$\begin{aligned}
 \Delta\mathbf{S}_{1/4,1\bar{1}0}(\mathbf{B}) &= 0, \\
 \Delta\mathbf{S}_{2,1\bar{1}0}(\mathbf{B}) &= -\Delta\mathbf{S}_{3,1\bar{1}0}(\mathbf{B}), \\
 \Delta\mathbf{S}_{2,11\bar{2}}(\mathbf{B}) &= \Delta\mathbf{S}_{3,11\bar{2}}(\mathbf{B}).
 \end{aligned} \tag{A7}$$

Hence, each spin change is

$$\begin{aligned}
 \Delta\mathbf{S}_{1\perp} &= s_1(B)\hat{e}_{11\bar{2}}, \\
 \Delta\mathbf{S}_{2\perp} &= t_1(B)\hat{e}_{1\bar{1}0} + s_2(B)\hat{e}_{11\bar{2}}, \\
 \Delta\mathbf{S}_{3\perp} &= -t_1(B)\hat{e}_{1\bar{1}0} + s_2(B)\hat{e}_{11\bar{2}}, \\
 \Delta\mathbf{S}_{4\perp} &= s_4(B)\hat{e}_{11\bar{2}},
 \end{aligned} \tag{A8}$$

where s_i, t_i are the polynomials of B . The TM is

$$\mathbf{M}_\perp = s(B)\hat{e}_{11\bar{2}}, \quad (\text{A9})$$

where $s(B) = aB + bB^2 + cB^3 + \dots$ is polynomial of B .

Lastly, let us think of T_{2y} under $\mathbf{B} \parallel [111]$, Then, $P_1 = \{I\}$, $P_2 = \{\sigma_{10\bar{1}}\}$. The condition is given by,

$$\begin{aligned} \Delta\mathbf{S}_{1/3,10\bar{1}}(\mathbf{B}) &= \Delta\mathbf{S}_{1/3,10\bar{1}}(-\mathbf{B}), \\ \Delta\mathbf{S}_{1/3,1\bar{2}1}(\mathbf{B}) &= -\Delta\mathbf{S}_{1/3,1\bar{2}1}(-\mathbf{B}), \\ \Delta\mathbf{S}_{2,10\bar{1}}(\mathbf{B}) &= \Delta\mathbf{S}_{4,10\bar{1}}(-\mathbf{B}), \\ \Delta\mathbf{S}_{2,1\bar{2}1}(\mathbf{B}) &= -\Delta\mathbf{S}_{4,1\bar{2}1}(-\mathbf{B}). \end{aligned} \quad (\text{A10})$$

Each spin change becomes

$$\begin{aligned} \Delta\mathbf{S}_{1\perp} &= (b_1B^2 + \dots)\hat{e}_{10\bar{1}} + (d_1B + f_1B^3 + \dots)\hat{e}_{1\bar{2}1}, \\ \Delta\mathbf{S}_{2\perp} &= (a_2B + b_2B^2 + c_2B^3 + \dots)\hat{e}_{10\bar{1}} \\ &\quad + (d_2B + e_2B^2 + f_2B^3 + \dots)\hat{e}_{1\bar{2}1}, \\ \Delta\mathbf{S}_{3\perp} &= (b_3B^2 + \dots)\hat{e}_{10\bar{1}} + (d_3B + f_3B^3 + \dots)\hat{e}_{1\bar{2}1}, \\ \Delta\mathbf{S}_{4\perp} &= (-a_2B + b_2B^2 - c_2B^3 + \dots)\hat{e}_{10\bar{1}} \\ &\quad + (d_2B - e_2B^2 + f_2B^3 + \dots)\hat{e}_{1\bar{2}1}, \end{aligned} \quad (\text{A11})$$

Thus, the TM is

$$\mathbf{M}_\perp = (bB^2 + \dots)\hat{e}_{10\bar{1}} + (dB + fB^3 + \dots)\hat{e}_{1\bar{2}1}. \quad (\text{A12})$$

In fact, we can do the same procedure for all symmetries in the MPG. However, because any symmetries other than P_1 and P_2 change the field direction, they does not give further physical meanings to the field dependence of TM. For example, under AIAO and $\mathbf{B} \parallel [110]$, recall that from $P_1 = \{I, \sigma_{1\bar{1}0}T\}$ and $P_2 = \{C_{2z}, \sigma_{110}T\}$, we have the following form of transverse spin change.

$$\begin{aligned} \Delta\mathbf{S}_{1\perp}(\mathbf{B}) &= g_1(\mathbf{B})\hat{z}, \\ \Delta\mathbf{S}_{2\perp}(\mathbf{B}) &= f_2^{even}(\mathbf{B})\hat{e}_{1\bar{1}0} + g_2^{even}(\mathbf{B})\hat{z}, \\ \Delta\mathbf{S}_{3\perp}(\mathbf{B}) &= -f_2^{even}(\mathbf{B})\hat{e}_{1\bar{1}0} + g_2^{even}(\mathbf{B})\hat{z}, \\ \Delta\mathbf{S}_{4\perp}(\mathbf{B}) &= g_1(-\mathbf{B})\hat{z}, \end{aligned} \quad (\text{A13})$$

where $f^{even}(\mathbf{B}) = f^{even}(-\mathbf{B})$. So the form of TM is $\Delta\mathbf{S}_{tot,\perp}(\mathbf{B}) = g^{even}(\mathbf{B})\hat{z}$.

We can apply $C_3 \notin P_1, P_2$ which is in the MPG of AIAO. Then, the condition is

$$\begin{aligned} \Delta\mathbf{S}_{1,1\bar{1}0}(\mathbf{B}) &= \Delta\mathbf{S}_{1,01\bar{1}}(C_3\mathbf{B}), \\ \Delta\mathbf{S}_{1,z}(\mathbf{B}) &= \Delta\mathbf{S}_{1,x}(C_3\mathbf{B}), \\ \Delta\mathbf{S}_{2,1\bar{1}0}(\mathbf{B}) &= \Delta\mathbf{S}_{3,01\bar{1}}(C_3\mathbf{B}), \\ \Delta\mathbf{S}_{2,z}(\mathbf{B}) &= \Delta\mathbf{S}_{3,x}(C_3\mathbf{B}), \\ \Delta\mathbf{S}_{3,1\bar{1}0}(\mathbf{B}) &= \Delta\mathbf{S}_{4,01\bar{1}}(C_3\mathbf{B}), \\ \Delta\mathbf{S}_{3,z}(\mathbf{B}) &= \Delta\mathbf{S}_{4,x}(C_3\mathbf{B}), \\ \Delta\mathbf{S}_{4,1\bar{1}0}(\mathbf{B}) &= \Delta\mathbf{S}_{2,01\bar{1}}(C_3\mathbf{B}), \\ \Delta\mathbf{S}_{4,z}(\mathbf{B}) &= \Delta\mathbf{S}_{2,x}(C_3\mathbf{B}). \end{aligned} \quad (\text{A14})$$

The conditions give,

$$\begin{aligned} \Delta\mathbf{S}_{1\perp}(C_3\mathbf{B}) &= g_1(\mathbf{B})\hat{x}, \\ \Delta\mathbf{S}_{2\perp}(C_3\mathbf{B}) &= g_1(-\mathbf{B})\hat{x}, \\ \Delta\mathbf{S}_{3\perp}(C_3\mathbf{B}) &= f_2^{even}(\mathbf{B})\hat{e}_{01\bar{1}} + g_2^{even}(\mathbf{B})\hat{x}, \\ \Delta\mathbf{S}_{4\perp}(C_3\mathbf{B}) &= -f_2^{even}(\mathbf{B})\hat{e}_{01\bar{1}} + g_2^{even}(\mathbf{B})\hat{x}, \end{aligned} \quad (\text{A15})$$

so $\Delta\mathbf{S}_{tot,\perp}(C_3\mathbf{B}) = g^{even}(\mathbf{B})\hat{x}$. The physical meaning of this is just the rotation of \mathbf{B} and \mathbf{M}_\perp .

Appendix B: Cluster Magnetic Multipoles in crystals

The cluster magnetic multipoles (CMMs) are the quantification of a generic magnetic ordering, just like the magnetization.³ In a magnetic unit cell, a spin cluster is defined as the group of atoms connected by the symmorphic symmetries. Therefore, there can be several spin clusters in a magnetic unit cell. The spin clusters are connected each other by the translational or non-symmorphic symmetries.

In a spin cluster a , one can define a CMM with rank p ,

$$M_{pq}^a = \sqrt{\frac{4\pi}{2p+1}} \sum_{i=1}^{N_a} \nabla(r_i^p Y_{pq}) \cdot \mathbf{m}_i, \quad (\text{B1})$$

where N_a is the number of atoms in the spin cluster, r_i is the position of i -th atom, Y_{pq} is the rank- p spherical harmonics, and \mathbf{m}_i is the magnetic moment at i -th atom. After we calculate M_{pq} , we classified them into the bases of irreducible representations (IRREPs) of T_d , O_h , and D_{3h} point group. We are aware of the cluster magnetic toroidal multipoles, but we consider the response to the magnetic field only, so we do not consider this. We adopt the magnetic unit cell of pyrochlore oxides, Mn_3Ir , and CsMnBr_3 for each point group, whose structures are in the manuscript.

Each magnetic unit cell of pyrochlore oxides, Mn_3Ir , and CsMnBr_3 is composed of a single spin cluster. Note that the number of degrees of freedom in a spin cluster is 12 (4 sublattices with 3 axes) in pyrochlore oxides, 18 (6 sublattices with 3 axes) in CsMnBr_3 , 9 (3 sublattices with 3 axes) in Mn_3Ir . Pyrochlore oxides can carry magnetic dipoles, octupoles, and dotriacontapoles. Mn_3Ir carries magnetic dipoles and octupoles. CsMnBr_3 carries magnetic dipoles, octupoles, dotriacontapoles, and 128-poles. Furthermore, we calculate the magnetic point group for each CMM, and determine whether TM exists or not, as we explain in the manuscript. All results are in the Tables S1-S3, and Figs. S1-S3.

Rank	CMM	[100]	[010]	[001]	[110]	[1 $\bar{1}$ 0]	[101]	[$\bar{1}$ 01]	[011]	[01 $\bar{1}$]	[111]	[1 $\bar{1}\bar{1}$]	[$\bar{1}$ 1 $\bar{1}$]	[$\bar{1}\bar{1}$ 1]
Octupole	A_2	×	×	×	O	O	O	O	O	O	×	×	×	×
	T_x^1	×	O	O	O	O	O	O	O	O	O	O	O	O
	T_y^1	O	×	O	O	O	O	O	O	O	O	O	O	O
	T_z^1	O	O	×	O	O	O	O	O	O	O	O	O	O
	T_x^2	×	O	O	O	O	O	O	×	×	O	O	O	O
	T_y^2	O	×	O	O	O	×	×	O	O	O	O	O	O
	T_z^2	O	O	×	×	×	O	O	O	O	O	O	O	O
Dotriacontapole	E_1	×	×	×	O	O	O	O	O	O	O	O	O	O
	E_2	×	×	×	×	×	O	O	O	O	O	O	O	O

TABLE S1. The presence (O) or absence (X) of TM for all possible magnetic structures in the pyrochlore lattice with the point group T_d under various field directions.

Rank	CMM	[100]	[010]	[001]	[110]	[1 $\bar{1}$ 0]	[101]	[$\bar{1}$ 01]	[011]	[01 $\bar{1}$]	[111]	[1 $\bar{1}\bar{1}$]	[$\bar{1}$ 1 $\bar{1}$]	[$\bar{1}\bar{1}$ 1]
Octupole	A'_1	O	×	×	O	O	O	O	O	O	O	O	O	O
	A'_2	O	O	×	O	O	O	O	O	O	O	O	O	O
	A''_2	×	O	×	O	O	O	O	O	O	O	O	O	O
	E'_x	×	×	×	O	O	O	O	O	O	O	O	O	O
	E'_y	O	O	×	O	O	O	O	O	O	O	O	O	O
	E''_x	×	O	O	O	O	O	O	O	O	O	O	O	O
	E''_y	O	×	O	O	O	O	O	O	O	O	O	O	O
Dotriacontapole	$2E'_x$	×	×	×	O	O	O	O	O	O	O	O	O	O
	$2E'_y$	O	O	×	O	O	O	O	O	O	O	O	O	O
	E''_x	×	O	O	O	O	O	O	O	O	O	O	O	O
	E''_y	O	×	O	O	O	O	O	O	O	O	O	O	O
128-pole	A'_1	×	×	×	O	O	O	O	O	O	O	O	O	O
	A''_1	O	×	×	O	O	O	O	O	O	O	O	O	O

TABLE S2. The presence (O) or absence (X) of TM for all possible magnetic structures in CsMnBr₃ with the point group D_{3d} under various field directions. The ground state is A'_1 -128-pole.

Rank	CMM	[100]	[010]	[001]	[110]	[1 $\bar{1}$ 0]	[101]	[$\bar{1}$ 01]	[011]	[01 $\bar{1}$]	[111]	[1 $\bar{1}\bar{1}$]	[$\bar{1}$ 1 $\bar{1}$]	[$\bar{1}\bar{1}$ 1]
Octupole	T_x^1	×	O	O	O	O	O	O	O	O	O	O	O	O
	T_y^1	O	×	O	O	O	O	O	O	O	O	O	O	O
	T_z^1	O	O	×	O	O	O	O	O	O	O	O	O	O
	T_x^2	×	O	O	O	O	O	O	×	×	O	O	O	O
	T_y^2	O	×	O	O	O	×	×	O	O	O	O	O	O
	T_z^2	O	O	×	×	×	O	O	O	O	O	O	O	O
Ground state	$T_x^1 = T_y^1 = T_z^1$	O	O	O	O	O	O	O	O	O	×	O	O	O

TABLE S3. The presence (O) or absence (X) of TM for all possible magnetic structures in Mn₃Ir with the point group O_h under various field directions.

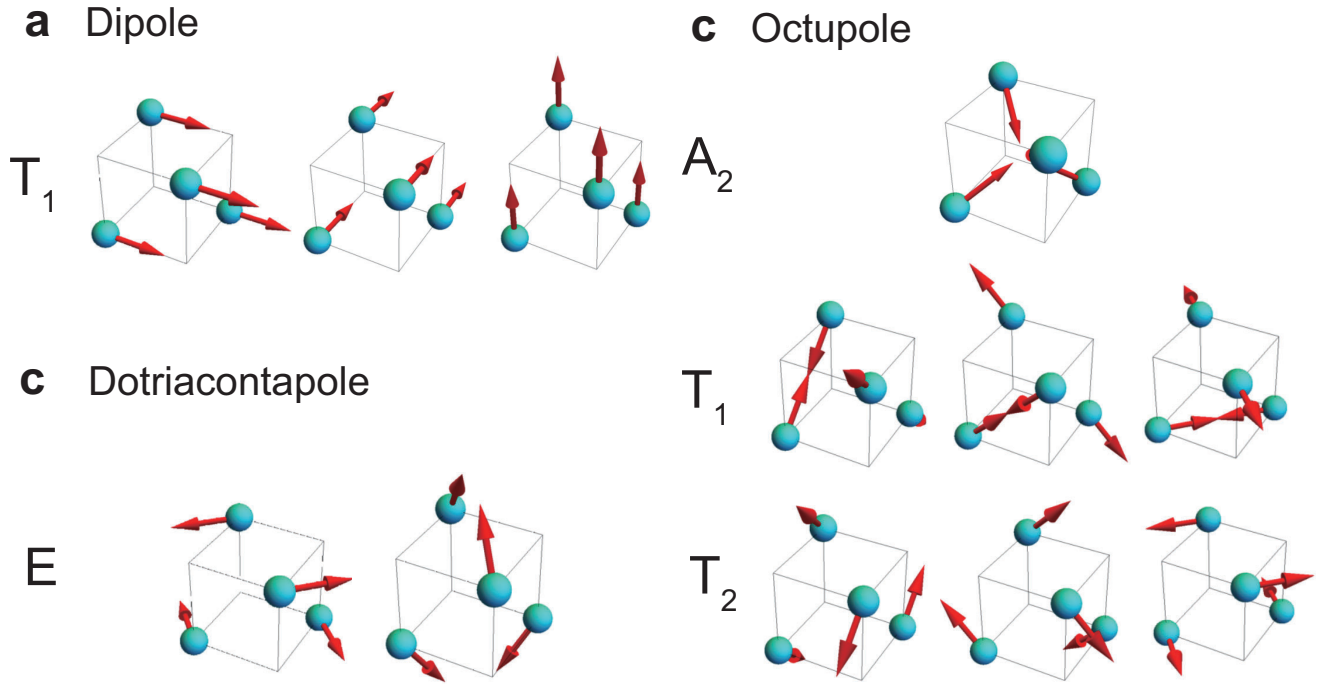


FIG. S1. CMMs of pyrochlore oxides. (a) Dipoles, (b) octupoles, and (c) dotriacontapoles.

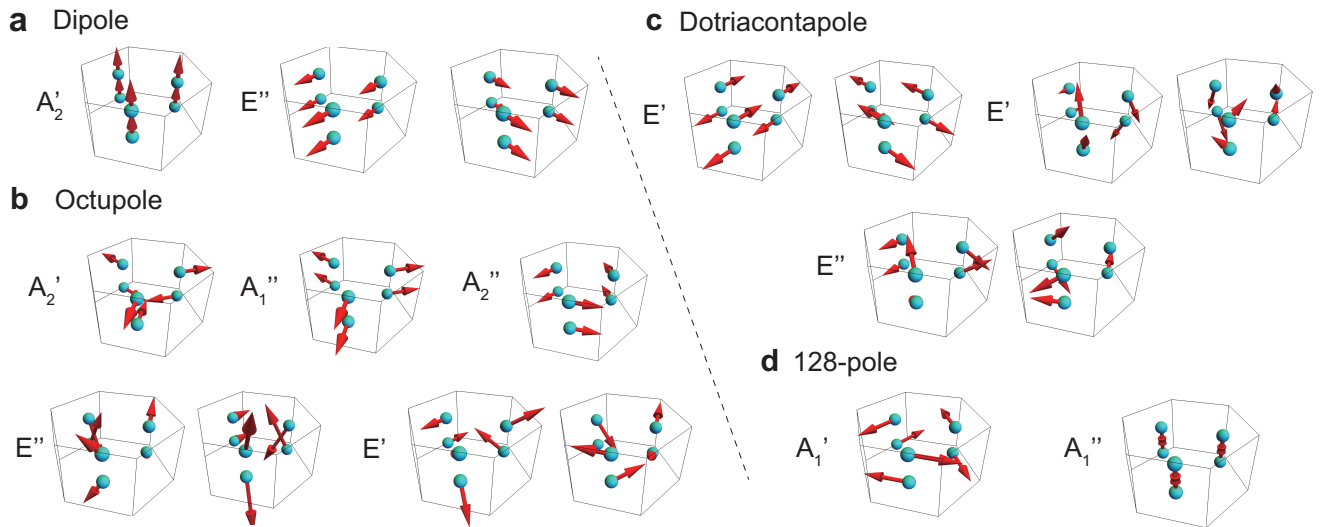
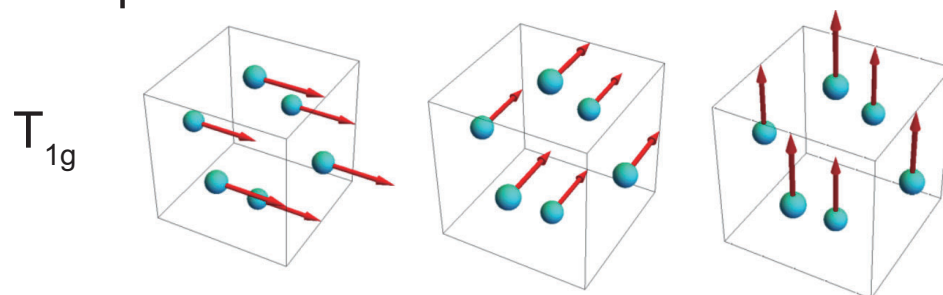


FIG. S2. CMMs of CsMnBr_3 . (a) Dipoles, (b) octupoles, (c) dotriacontapoles, and (d) 128-poles.

a Dipole



b Octupole

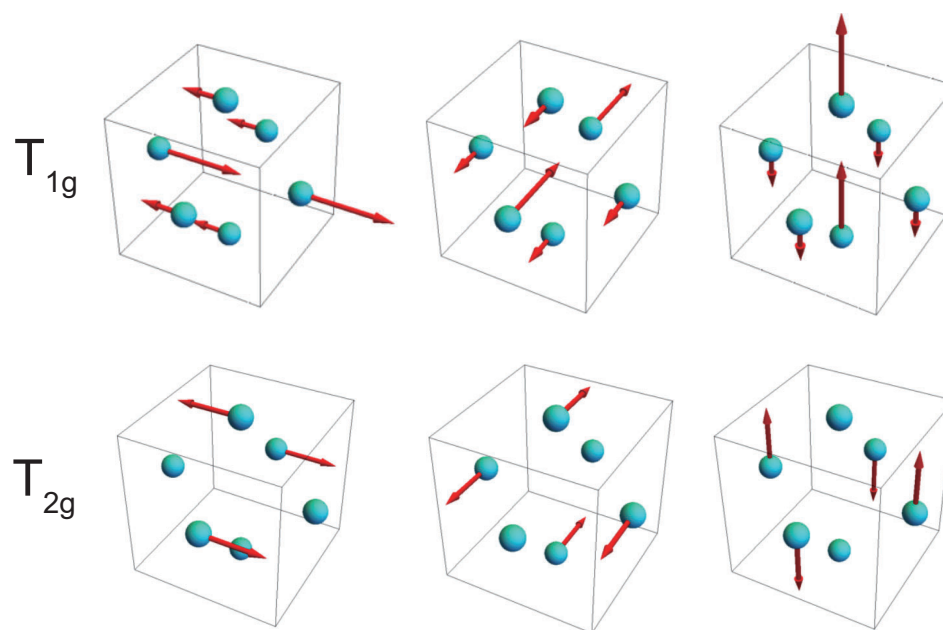


FIG. S3. CMMs of Mn_3Ir . (a) Dipoles and (b) octupoles.

Appendix C: The numerical computations of \mathbf{M}_\perp

Here, we perform numerical computations of \mathbf{M}_\perp considering general Hamiltonians for classical spins on the pyrochlore lattice given by

$$H = H_J + H_{ani} - \sum_a \mathbf{B} \cdot \mathbf{S}_a, \quad (\text{C1})$$

where H_J indicate the isotropic Heisenberg spin Hamiltonian, and $H_{ani} = H_{DMI}, H_{SIA}, H_{DI}$ indicates the anisotropic spin Hamiltonian including Dzyaloshinskii-Moriya interaction (DMI),²⁷ single-ion anisotropy (SIA),¹⁸ and dipolar interaction (DI),²⁶ respectively. Their explicit forms are

$$H_J = J \sum_{\langle ab \rangle} \mathbf{S}_a \cdot \mathbf{S}_b, \quad (\text{C2})$$

$$H_{DMI} = D \sum_{\langle ab \rangle} \hat{\mathbf{D}}_{ab} \cdot (\mathbf{S}_a \times \mathbf{S}_b), \quad (\text{C3})$$

$$H_{SIA} = A \sum_a (\mathbf{S}_a \cdot \mathbf{n}_a)^2, \quad (\text{C4})$$

$$H_{DI} = J_{DI} \sum_{\langle ab \rangle} [\mathbf{S}_a \cdot \mathbf{S}_b - 3(\mathbf{S}_a \cdot \mathbf{r}_{ab})(\mathbf{S}_b \cdot \mathbf{r}_{ab})], \quad (\text{C5})$$

where $J > 0$ is the antiferromagnetic Heisenberg exchange interaction, D (A) is the strength of DMI (SIA), and J_{DI} indicates the strength of the DI. Also, $\hat{\mathbf{D}}_{ab}$ is the unit vector of DMI, \mathbf{n}_a is the unit vector along the local z -axis of the spin \mathbf{S}_a , and \mathbf{r}_{ab} is the normalized displacement vector between a -th and b -th sites.

When we calculate the ground state, we begin from a random spin configuration and make an iterative approach. For given spin configuration and Hamiltonian H , the effective field at site a is given by $\mathbf{h}_a = -\frac{\partial H}{\partial \mathbf{S}_a}$. Then, we make the spin evolves to the direction of its mean-field,

$$\mathbf{S}_a \rightarrow \frac{\mathbf{S}_a + c\mathbf{h}_a}{\|\mathbf{S}_a + c\mathbf{h}_a\|} \quad (\text{C6})$$

where c is the parameter given by hand. The ground state has the lowest energy among the converged spin configuration.⁴²

Depending on the type of the anisotropic spin interactions, various AFM ground states with distinct CMMs can appear.^{18,26,27} For example, suppose that $H = H_J + H_{DMI}$. Then, for $D > 0$, the ground state is an A_2 -octupole, while for $D < 0$, the ground state is an E -dotriacontapole or a T_1 -octupole. On the other hand, if $H = H_J + H_{SIA}$, for $A < 0$, the ground state is A_2 -octupole, while for $A > 0$, the ground state is an E -dotriacontapole or a T_2 -octupole.

For each spin Hamiltonian on the pyrochlore lattice, we compute $\mathbf{M}_\perp \equiv \frac{1}{4} \sum_{i=1}^4 \langle \mathbf{S}_{i,\perp} \rangle$ as a function of \mathbf{B} . The parameters are chosen as $J = |D| = |A| = 1$ for numerical computations.⁴²

Let us first consider the A_2 -order of $H_J + H_{DMI}$ and $H_J + H_{SIA}$. The relevant $\mathbf{M}_\perp \parallel \hat{z}$ under $\mathbf{B} \parallel [110]$ is plotted in Figs. S4a-b, respectively. One can clearly observe $\mathbf{M}_\perp \propto B^2$ for both cases.

Next we consider $E = (E_1, E_2)$ -order of $H_J + H_{DMI}$ and $H_J + H_{SIA}$. Here we choose E_2 -order ($E = (0, 1)$) as an initial ground state configuration, compute $\mathbf{M}_\perp \parallel [112]$ under $\mathbf{B} \parallel [111]$, and show the result in Figs. S4c-d. For both DMI and SIA cases, $\mathbf{M}_\perp = 0$. On the other hand, we choose E_1 -order ($E = (1, 0)$) as a ground state, compute $\mathbf{M}_\perp^{calc} \parallel [112]$ under $\mathbf{B} \parallel [111]$, and show the result in Fig. S4e-f. For DMI case, $\mathbf{M}_\perp^{calc} = 0$, but for SIA case, $\mathbf{M}_\perp^{calc} \propto B$. We choose $E(\pi/4) = (1/\sqrt{2}, 1/\sqrt{2})$ -order as a ground state, compute $\mathbf{M}_\perp \parallel [112]$ under $\mathbf{B} \parallel [111]$, and show the result in Fig. S4g. For both $H_J + H_{DMI}$ and $H_J + H_{SIA}$, $\mathbf{M}_\perp^{calc} = 0$. In generic $E(\alpha)$ -order ($E = (\sin \alpha, \cos \alpha)$), TM vanishes for both cases.

Lastly, we consider T_{2y} -order of $H_J + H_{DI}$. Here we choose T_{2y} -order as a ground state. The resulting $\mathbf{M}_\perp^{calc} \parallel [121]$ is in Fig. S4h. One can easily note that $\mathbf{M}_\perp^{calc} \propto B^3$.

Appendix D: Hubbard model for pyrochlore oxides

The Hubbard model for pyrochlore oxides is,

$$H = H_0 + H_U^{MF} + H_B, \quad (\text{D1})$$

where

$$H_0 = \sum_{\langle ij \rangle} c_i^\dagger (t_1 + it_2 \vec{d}_{ij} \cdot \vec{\sigma}) c_j + \sum_{\langle\langle ij \rangle\rangle} c_i^\dagger (t'_1 + i(t'_2 \vec{R}_{ij} + t'_3 \vec{D}_{ij})) c_j, \quad (\text{D2})$$

is the kinetic Hamiltonian,

$$H_U^{MF} = -U \sum_i (\langle \vec{j}_i \rangle \cdot \vec{j}_i - \langle \vec{j}_i \rangle^2), \quad (\text{D3})$$

is the mean-field approximated Hubbard repulsion, and

$$H_B = - \sum_i \vec{B} \cdot \vec{j}_i, \quad (\text{D4})$$

is the Zeeman coupling.^{24,40} Note that $\vec{j}_i = \frac{1}{2} \sum_i c_i^\dagger \vec{\sigma} c_i$.

The parameter we used are

$$\begin{aligned} t_1 &= \frac{130}{243} t_{oxy} + \frac{17}{324} t_\sigma - \frac{79}{243} t_\pi, \\ t_2 &= \frac{28}{243} t_{oxy} + \frac{15}{243} t_\sigma - \frac{40}{243} t_\pi, \\ t'_1 &= \frac{233}{2916} t'_\sigma - \frac{407}{2187} t'_\pi, \\ t'_2 &= \frac{1}{1458} t'_\sigma + \frac{220}{2187} t'_\pi, \\ t'_3 &= \frac{25}{1458} t'_\sigma + \frac{460}{2187} t'_\pi, \end{aligned} \quad (\text{D5})$$

where t_{oxy} is the oxygen mediated nearest neighbor (NN) hopping, t_σ, t_π are the direct-overlap NN hopping, and t'_σ, t'_π are the direct-overlap next NN hopping. We set $t_{oxy} = 1$, $t_\sigma = -0.8 t_{oxy}$, $t_\pi = -2 t_\sigma / 3$, and $t'_{\sigma,\pi} = 0.08 t_{\sigma,\pi}$. The

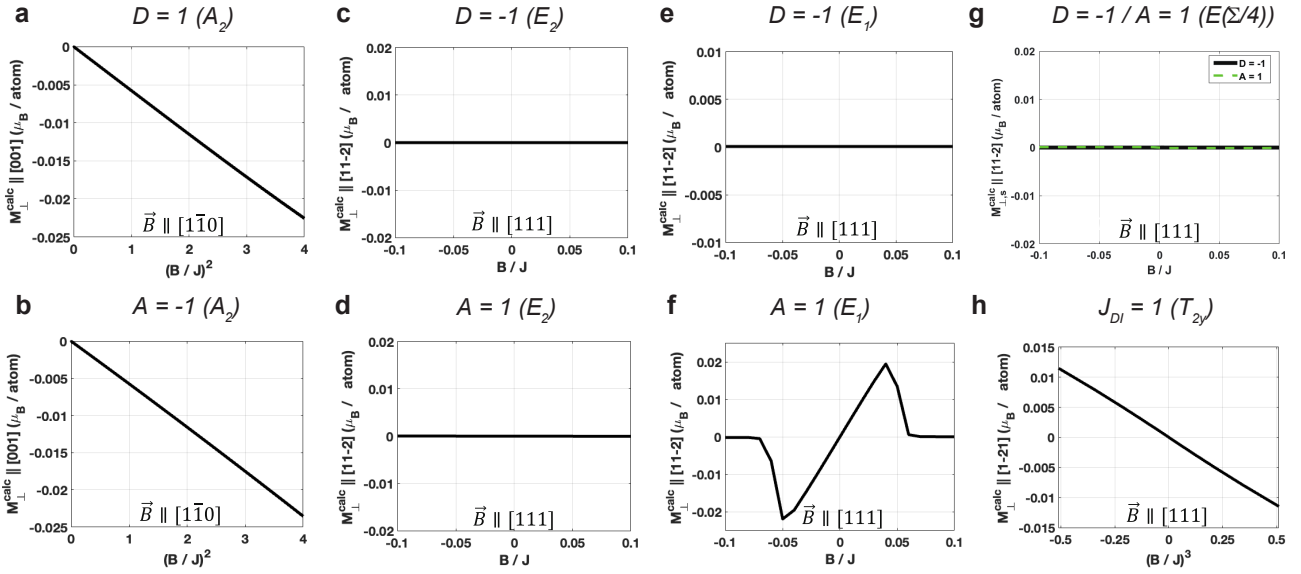


FIG. S4. Numerical computation of M_{\perp}^{calc} from spin Hamiltonian. (a-b) M_{\perp}^{calc} for A_2 -order with (a) $D = 1$ and (b) $A = -1$ under $\mathbf{B} \parallel [1\bar{1}0]$. $M_{\perp}^{\text{calc}} \propto B^2$ for both cases. (c-d) M_{\perp}^{calc} for E_2 -order with (c) $D = -1$ and (d) $A = 1$ under $\mathbf{B} \parallel [111]$. $M_{\perp}^{\text{calc}} = 0$ for both cases. (e-f) M_{\perp}^{calc} for E_1 -order with (e) $D = -1$ and (f) $A = 1$ under $\mathbf{B} \parallel [111]$. In (e), $M_{\perp}^{\text{calc}} = 0$, whereas in (f), $M_{\perp}^{\text{calc}} \propto B$. (g) M_{\perp}^{calc} for $E(\pi/4)$ -order with $D = -1$ (black solid line) and $A = 1$ (black circles). $M_{\perp}^{\text{calc}} = 0$. (h) M_{\perp}^{calc} for T_{2y} -order with $J_{D1} = 1$. $M_{\perp}^{\text{calc}} \propto B^3$.

Hubbard interaction $U = 1.485$. Also, the Dzyaloshinskii-Moriya (DM) vectors are defined as

$$\begin{aligned}\vec{d}_{ij} &= 2\vec{a}_{ij} \times \vec{b}_{ij}, \\ \vec{R}_{ij} &= \vec{b}_{ik} \times \vec{b}_{ki}, \\ \vec{D}_{ij} &= \vec{d}_{ik} \times \vec{d}_{kj}.\end{aligned}\quad (\text{D6})$$

where \vec{b}_{ij} is the vector from i -th to j -th sublattices, \vec{a}_{ij} is the vector that points from the center of a unit cell to the middle of $\langle ij \rangle$ bond, and k -th sublattice is the shared neighbor of i -th and j -th sublattices. We assume that the electric field is applied along $[1\bar{1}0]$ and the magnetic field is applied in the $[111]$ plane and at angle θ by $[1\bar{1}0]$. We fix $B/t_{\text{oxy}} = 0.03$, changing $\theta = 0$ to 2π . We calculate the self-consistent ground state by using $30 \times 30 \times 30$ k -point mesh.

Using the acquired self-consistent ground state, we compute the AHC and PHC. The formula of AHC and PHC are given by^{35,41}

$$\sigma_{xy}^{\text{AHE}} = \frac{e^2}{\hbar} \sum_n \int \frac{d^3k}{(2\pi)^3} \Omega_n^z(\mathbf{k}) f(\epsilon_n(\mathbf{k})), \quad (\text{D7})$$

$$\begin{aligned}\sigma_{xy}^{\text{PHE}} &= e^2 \int \frac{d^3k}{(2\pi)^3} D\tau \left(-\frac{\partial f}{\partial \epsilon} \right) \left(v_x + \frac{eB_x}{\hbar} (\mathbf{v}_k \cdot \boldsymbol{\Omega}_k) \right) \\ &\quad \times \left(v_y + \frac{eB_y}{\hbar} (\mathbf{v}_k \cdot \boldsymbol{\Omega}_k) \right),\end{aligned}\quad (\text{D8})$$

where $\boldsymbol{\Omega}_k$ is the Berry curvature, \mathbf{v}_k is the group velocity, $f(\epsilon)$ is the Fermi-Dirac distribution, τ is the relaxation time, $D = (1 + (e/\hbar)\mathbf{B} \cdot \boldsymbol{\Omega}_k)^{-1}$ is the phase volume change because of Berry curvature. We take $e = \hbar = a = \tau = 1$, where a is the lattice constant.

Appendix E: Details in microscopic origin of TM

1. Without anisotropy

When there is no anisotropy, the spin interaction is given by $H = H_J$ with $J > 0$. The ground state of H_J is highly degenerate. When we consider the pyrochlore lattice, the Hamiltonian is

$$H_J = J \sum_{\langle ab \rangle} \mathbf{S}_a \cdot \mathbf{S}_b = 8JN_c M^2 - \frac{JN_c}{2} \sum_{a=1}^4 \mathbf{S}_a^2, \quad (\text{E1})$$

where N_c is the number of unit cell, $\mathbf{M} = \frac{1}{4} \sum_{a=1}^4 \mathbf{S}_a$ is the average magnetization. Physically, the classical spins have the same magnitude, $\mathbf{S}_a^2 = 1$ for all a s, so the last term is a constant as $\sum_{a=1}^4 \mathbf{S}_a^2 = 4$. Then,

$$H_J = 8JN_c M^2. \quad (\text{E2})$$

The ground state can be any antiferromagnetic states, i.e. $\mathbf{M} = 0$.

When we add the magnetic field, the Hamiltonian is

$$\begin{aligned}H &= H_J + H_B \\ &= 8JN_c M^2 - 4N_c \mathbf{B} \cdot \mathbf{M} - \frac{JN_c}{2} \sum_{a=1}^4 \mathbf{S}_a^2,\end{aligned}\quad (\text{E3})$$

Again, the last term is constant, the Hamiltonian becomes

$$H = 8JN_c \left(\mathbf{M} - \frac{\mathbf{B}}{4J} \right)^2. \quad (\text{E4})$$

The energy minimum is $H = 0$ at

$$\mathbf{M} = \frac{\mathbf{B}}{4J}. \quad (\text{E5})$$

Since the magnetization is parallel to \mathbf{B} , the TM vanishes.

2. Single-ion anisotropy ($A > 0$)

Next, let us add the SIA,

$$H = H_J + H_{SIA} + H_B, \quad (\text{E6})$$

$$= J \sum_{\langle ab \rangle} \mathbf{S}_a \cdot \mathbf{S}_b + A \sum_a (\mathbf{S}_a \cdot \mathbf{n}_a)^2 - \sum_a \mathbf{B} \cdot \mathbf{S}_a, \quad (\text{E7})$$

where $J > 0$ and $A > 0$. For H_{SIA} , the energy minimum requires

$$\mathbf{S}_a \cdot \mathbf{n}_a = 0, \quad (\text{E8})$$

for each $a = 1, 2, 3, 4$, separately. This forces each spin to lying in its local xy -plane, so reduces the ground state manifold. The red arrows are spins \mathbf{S}_a , the yellow arrows are the hard axes \mathbf{n}_a , and the yellow planes are the local- xy plane. Thus, for the full Hamiltonian $H = H_J + H_{SIA} + H_B$, the energy minimum requires

$$\mathbf{M} = \frac{\mathbf{B}}{4J}, \quad \mathbf{S}_a \cdot \mathbf{n}_a = 0. \quad (\text{E9})$$

When $\mathbf{B} = 0$, the ground state is either E -dotriacontapole or T_2 -octupole, where all spins are lying on their local xy -plane. E -dotriacontapole has E_1 and E_2 -orders. There are several ground states. The first ground state is generally represented by $E(\alpha) = (E_1 = \sin \alpha, E_2 = \cos \alpha)$ -order. The spins in $E(\alpha)$ -order are

$$\mathbf{S}_a = \cos \alpha \hat{x}_a + \sin \alpha \hat{y}_a \quad (\text{E10})$$

where

$$\begin{aligned} \hat{x}_1 &= [\bar{1}10], \hat{x}_2 = [110], \hat{x}_3 = [\bar{1}\bar{1}0], \hat{x}_4 = [\bar{1}10], \\ \hat{y}_1 &= [11\bar{2}], \hat{y}_2 = [1\bar{1}2], \hat{y}_3 = [\bar{1}12], \hat{y}_4 = [\bar{1}\bar{1}2], \\ \hat{z}_1 &= [111], \hat{z}_2 = [1\bar{1}\bar{1}], \hat{z}_3 = [\bar{1}1\bar{1}], \hat{z}_4 = [\bar{1}\bar{1}1]. \end{aligned} \quad (\text{E11})$$

Note that \hat{x}_a is the direction of spins in E_2 -order, and \hat{y}_a is that in E_1 -order.

The next type of ground state is $E + T_2(\alpha)$ -orders. There are three kinds of the orders. The first one is $E_1 + T_{2z}(\alpha)$ which is represented by

$$\mathbf{S}_a = d_a \cos \alpha \hat{x}_a + \sin \alpha \hat{y}_a \quad (\text{E12})$$

where $d_a = 1$ for $a = 1, 4$ and $d_a = -1$ for $a = 2, 3$. The spin configuration for $\alpha = 0$ is T_{2z} -order while that for $\alpha = \pi/2$ is E_1 -order. This means that when α increases two spins at $a = 2, 3$ in $E_1 + T_{2z}(\alpha)$ -order rotate oppositely from those spins in $E(\alpha)$ -order.

The next one is $E(\pi/6) + T_{2x}(\alpha)$ which is represented by

$$\mathbf{S}_a = e_a \cos \alpha \hat{x}'_a + \sin \alpha \hat{y}'_a \quad (\text{E13})$$

where $\hat{x}'_a = \frac{1}{2}\hat{x}_a - \frac{\sqrt{3}}{2}\hat{y}_a$, $\hat{y}'_a = \frac{\sqrt{3}}{2}\hat{x}_a + \frac{1}{2}\hat{y}_a$, $e_a = 1$ for $a = 1, 2$ and $e_a = -1$ for $a = 3, 4$. The spin configuration for $\alpha = 0$ is T_{2x} -order while that for $\alpha = \pi/2$ is $E(\pi/6)$ -order. This means that when α increases two spins at $a = 3, 4$ in $E(\pi/6) + T_{2x}(\alpha)$ -order rotate oppositely from those spins in $E(\alpha)$ -order.

The last one is $E(5\pi/6) + T_{2y}(\alpha)$ which is represented by

$$\mathbf{S}_a = f_a \cos \alpha \hat{x}''_a + \sin \alpha \hat{y}''_a \quad (\text{E14})$$

where $\hat{x}''_a = \frac{1}{2}\hat{x}_a + \frac{\sqrt{3}}{2}\hat{y}_a$, $\hat{y}''_a = -\frac{\sqrt{3}}{2}\hat{x}_a + \frac{1}{2}\hat{y}_a$, $f_a = 1$ for $a = 1, 3$ and $f_a = -1$ for $a = 2, 4$. The spin configuration for $\alpha = 0$ is T_{2y} -order while that for $\alpha = \pi/2$ is $E(5\pi/6)$ -order. This means that when α increases two spins at $a = 2, 4$ in $E(5\pi/6) + T_{2y}(\alpha)$ -order rotate oppositely from those spins in $E(\alpha)$ -order.

Please note that all ground state manifold is continuously degenerate without magnetic field. We take $E(\alpha)$ -order as a ground state for convenience, but the following results are the same as the other ground state manifolds as well.

When $\mathbf{B} \neq 0$, the stationary condition satisfying Eq. E9 usually exists, but not in a few cases. Because all spins are described by their polar and azimuthal angles (θ_a, ϕ_a) , the number of degrees of freedom is 8. As the number of equations in Eq. E9 is 7, the ground state exists in general. However, as we seek the stationary condition by a smooth deviation of (θ_a, ϕ_a) at small \mathbf{B} limit, the such state satisfying Eq. E9 may not exist depending on the initial spin configuration: for instance, $E(\pi/6 + n\pi/3)$ -orders. ($n \in \mathbb{Z}$)

For illustration, let us consider the case when the initial spin configuration is a E -dotriacontapole $E = (E_1, E_2)$ at $\mathbf{B} = 0$. In the case of E_2 -order with $\alpha = 0$, the configuration of each spin can be represented by

$$\begin{aligned} \mathbf{S}_a &= \sin\left(\frac{\pi}{2} + \theta_a\right) \cos(\phi_a) \hat{x}_a \\ &\quad + \sin\left(\frac{\pi}{2} + \theta_a\right) \sin(\phi_a) \hat{y}_a \\ &\quad + \cos\left(\frac{\pi}{2} + \theta_a\right) \hat{z}_a, \end{aligned} \quad (\text{E15})$$

where $\hat{x}_a, \hat{y}_a, \hat{z}_a$ are in Eq. E11. When $\theta_a, \phi_a = 0$, the spin configuration is the E_2 -order. To describe the deformation of the spin configuration under small \mathbf{B} , we expand \mathbf{S}_a up to the first order of angular variables as

$$\mathbf{S}_a = \hat{x}_a + \phi_a \hat{y}_a - \theta_a \hat{z}_a, \quad (\text{E16})$$

with which Eq. E9 become

$$\begin{aligned} \mathbf{S}_a \cdot \mathbf{n}_a &= -\theta_a = 0. \\ \mathbf{M} &= \frac{1}{4\sqrt{3}} [\phi_1 + \phi_2 - \phi_3 - \phi_4 - \theta_1 - \theta_2 + \theta_3 + \theta_4, \\ &\quad \phi_1 - \phi_2 + \phi_3 - \phi_4 - \theta_1 + \theta_2 - \theta_3 + \theta_4, \\ &\quad 2(-\phi_1 + \phi_2 + \phi_3 - \phi_4) - \theta_1 + \theta_2 + \theta_3 - \theta_4] \\ &= \frac{\mathbf{B}}{4J}. \end{aligned} \quad (\text{E17})$$

The solution of the first constraint equations is $\theta_a = 0$, which means that the SIA forces the spins to rotate in their local xy -planes. For $\mathbf{B} = [B_x, B_y, B_z]$, the solution of the second constraint equations can be written as

$$\begin{aligned}\phi_2 &= (-2\sqrt{3}B_y + \sqrt{3}B_z)/4J + \phi_1, \\ \phi_3 &= (-2\sqrt{3}B_x + \sqrt{3}B_z)/4J + \phi_1, \\ \phi_4 &= -\sqrt{3}(B_x + B_y)/2J + \phi_1.\end{aligned}\quad (\text{E18})$$

That is, the stationary condition satisfying Eq. E9 exists. Accordingly, the TM should vanish. We confirm that for a general $E(\alpha)$ -order case, the stationary condition satisfying Eq. E9 exists and thus the TM vanishes.

On the other hand, there are some cases that the stationary condition satisfying Eq. E9 does not exist. Considering the E_1 -order with $\alpha = \pi/2$, the configuration of each spin can be represented by

$$\begin{aligned}\mathbf{S}_a &= \sin(\frac{\pi}{2} + \theta_a) \cos(\frac{\pi}{2} + \phi_a) \hat{x}_a \\ &\quad + \sin(\frac{\pi}{2} + \theta_a) \sin(\frac{\pi}{2} + \phi_a) \hat{y}_a \\ &\quad + \cos(\frac{\pi}{2} + \theta_a) \hat{z}_a.\end{aligned}\quad (\text{E19})$$

Up to the first order of angular variables, we find

$$\mathbf{S}_a = -\phi_a \hat{x}_a + \hat{y}_a - \theta_a \hat{z}_a, \quad (\text{E20})$$

with which Eq. E9 becomes

$$\begin{aligned}\mathbf{S}_a \cdot \mathbf{n}_a &= -\theta_a = 0. \\ \mathbf{M} &= \frac{1}{6} [(3\sqrt{2}(-\phi_1 - \phi_2 + \phi_3 + \phi_4) \\ &\quad + 2\sqrt{3}(-\theta_1 - \theta_2 + \theta_3 + \theta_4)), \\ &\quad (3\sqrt{2}(\phi_1 - \phi_2 + \phi_3 - \phi_4) \\ &\quad + 2\sqrt{3}(-\theta_1 + \theta_2 - \theta_3 + \theta_4)), \\ &\quad \frac{-\theta_1 + \theta_2 + \theta_3 - \theta_4}{\sqrt{3}}] = \frac{\mathbf{B}}{4J}.\end{aligned}\quad (\text{E21})$$

Again, the SIA forces the condition $\theta_a = 0$. However, the second equations of ϕ_a does not have a solution when $B_z \neq 0$. The stationary condition satisfying Eq. E9 does not exist. Considering the threefold and twofold rotations in $H_J + H_{SIA}$, $\alpha = \pi/6 + n\pi$ does not have a solution when $B_x \neq 0$, $\alpha = 5\pi/6 + n\pi$ does not have a solution when $B_y \neq 0$, and $\alpha = \pi/2 + n\pi$ does not have a solution when $B_z \neq 0$.

For an arbitrary $E(\alpha)$ -order, the spin configuration is given by

$$\begin{aligned}\mathbf{S}_a &= \cos \theta_a \cos(\alpha + \phi_a) \hat{x}_a + \cos \theta_a \sin(\alpha + \phi_a) \hat{y}_a \\ &\quad - \sin \theta_a \hat{z}_a,\end{aligned}\quad (\text{E22})$$

Then, Eq. E9 gives

$$\begin{aligned}\mathbf{S}_a \cdot \mathbf{n}_a &= -\theta_a = 0, \\ \mathbf{M} &= \frac{\mathbf{B}}{4J} \\ &= \frac{1}{4} [\frac{1}{6} (\sqrt{6} \cos \alpha - 3\sqrt{2} \sin \alpha) (\phi_1 + \phi_2 - \phi_3 - \phi_4), \\ &\quad \frac{1}{6} (\sqrt{6} \cos \alpha + 3\sqrt{2} \sin \alpha) (\phi_1 - \phi_2 + \phi_3 - \phi_4), \\ &\quad - \sqrt{\frac{2}{3}} (\phi_1 - \phi_2 - \phi_3 + \phi_4) \cos \alpha].\end{aligned}\quad (\text{E23})$$

When $\mathbf{B} = B(b_x, b_y, b_z)$, the solution is given by $\theta_a = 0$ and

$$\begin{aligned}\phi_2 &= \phi_1 - \frac{\sqrt{3}B(2\sqrt{6}b_y - \sqrt{6}b_z - 3\sqrt{2}b_z \tan \alpha)}{4J \cos \alpha (\sqrt{3} + 3 \tan \alpha)}, \\ \phi_3 &= \phi_1 - \frac{\sqrt{3}B(2\sqrt{6}b_x - \sqrt{6}b_z + 3\sqrt{2}b_z \tan \alpha)}{4J \cos \alpha (\sqrt{3} - 3 \tan \alpha)}, \\ \phi_4 &= \phi_1 - \frac{3B(\sqrt{6}(b_x + b_y) + 3\sqrt{2}(b_x - b_y) \tan \alpha)}{2J \cos \alpha (\sqrt{3} + 3 \tan \alpha) (\sqrt{3} - 3 \tan \alpha)},\end{aligned}\quad (\text{E24})$$

where ϕ_1 is arbitrary. The solution does not exist when $\alpha = \pi/6 + n\pi/3$ where the denominator goes to 0.

In fact, there is a condition that $\alpha = \pi/6 + n\pi/3$ does not have a solution. For example, $\alpha = \pi/2 + n\pi$, the second equation of Eq. E23 becomes

$$\frac{\mathbf{B}}{J} = \frac{3\sqrt{2}}{6} [(\mp(\phi_1 + \phi_2 - \phi_3 - \phi_4), \pm(\phi_1 - \phi_2 + \phi_3 - \phi_4), 0)], \quad (\text{E25})$$

Therefore, whenever $B_z \neq 0$, the solution does not exist. Similarly, for $\alpha = \pi/6 + n\pi$ ($5\pi/6 + n\pi$), the solution does not exist whenever $B_x \neq 0$ ($B_y \neq 0$).

$E(\pi/6 + n\pi/3)$ -orders are special since all spins in the orders are either parallel or antiparallel to the projected \mathbf{B} onto local- xy plane simultaneously. For $E(\alpha \neq \pi/6 + n\pi/3)$ -orders, there are some spins not parallel to the projected \mathbf{B} . For example, in $E(\pi/3)$ -order,

$$\mathbf{S}_1 \parallel [10\bar{1}], \mathbf{S}_2 \parallel [101], \mathbf{S}_3 \parallel [\bar{1}01], \mathbf{S}_4 \parallel [\bar{1}0\bar{1}]. \quad (\text{E26})$$

Suppose that

$$\mathbf{B} = B(\cos \beta [10\bar{1}]/\sqrt{2} + \sin \beta [111]/\sqrt{3}), \quad (\text{E27})$$

then \mathbf{S}_1 is parallel to the projected \mathbf{B} onto its local- xy plane whenever $\beta \neq \pi/2 + n\pi$. However, for other spins, the projected \mathbf{B} onto spin a (\mathbf{B}_a^P) are

$$\begin{aligned}\mathbf{B}_2^P &= \cos \beta [101]/\sqrt{3} + (2\sqrt{3} \cos \beta + 3\sqrt{2} \sin \beta) [12\bar{1}]/18, \\ \mathbf{B}_3^P &= -\sin \beta [\bar{1}01]/\sqrt{3} + (\cos \beta) [121]/3\sqrt{3}, \\ \mathbf{B}_4^P &= -\cos \beta [\bar{1}0\bar{1}]/\sqrt{3} + (-2\sqrt{3} \cos \beta + 3\sqrt{2} \sin \beta) [1\bar{2}1]/18,\end{aligned}\quad (\text{E28})$$

These are not parallel to $E(\pi/3)$ -order in Eq. E26 generally.

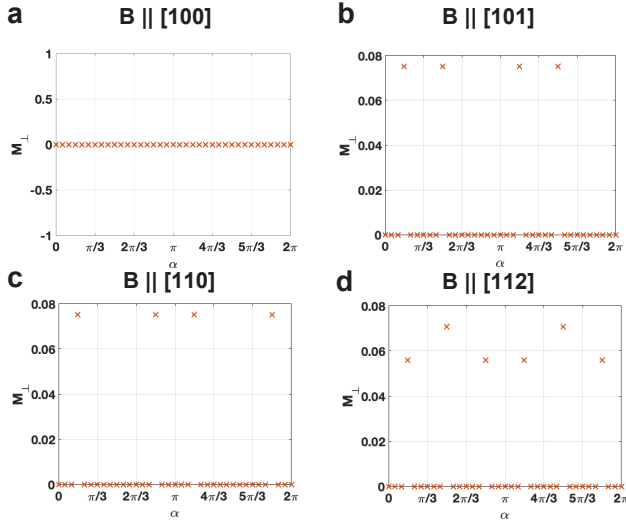


FIG. S5. TM M_{\perp} for $E(\alpha)$ -order with SIA under (a) $\mathbf{B} \parallel [100]$, (b) $\mathbf{B} \parallel [101]$, (c) $\mathbf{B} \parallel [110]$ and (d) $\mathbf{B} \parallel [112]$.

However, when $\mathbf{B} \parallel [001]$, the projected \mathbf{B} on each local- xy plane is

$$\mathbf{B}_1^P \parallel [\bar{1}\bar{1}2], \mathbf{B}_2^P \parallel [1\bar{1}2], \mathbf{B}_3^P \parallel [\bar{1}12], \mathbf{B}_4^P \parallel [112] \quad (\text{E29})$$

All projected magnetic fields are either parallel or antiparallel to E_1 -order ($E(\pi/2), E(3\pi/2)$). Hence, whenever $B_z \neq 0$, all spins deviate from local- xy planes. Similarly, for $\mathbf{B} \parallel [100]$, all projected magnetic fields are along $E(\pi/6)$ or $E(7\pi/6)$, and for $\mathbf{B} \parallel [010]$, all projected magnetic fields are along $E(5\pi/6)$ or $E(11\pi/6)$. Hence, all spins deviate from local- xy planes whenever $B_x \neq 0$ for $E(\pi/6)$ and $E(7\pi/6)$, and whenever $B_y \neq 0$ for $E(5\pi/6)$ and $E(11\pi/6)$.

We can obtain (θ_a, ϕ_a) of the stationary condition in series of $B = |\mathbf{B}|$ in E_1 -order by the derivative of Hamiltonian,

$$\frac{\partial H}{\partial \theta_a} = 0, \quad \frac{\partial H}{\partial \phi_a} = 0. \quad (\text{E30})$$

Up to the first order of B ,

$$\begin{aligned} \theta_1 = \theta_4 = -\theta_2 = -\theta_3 &= \frac{B}{6A + 4J}, \\ \phi_1 = \phi_4 &= 0, \\ \phi_2 = -\phi_3 &= -\frac{B}{\sqrt{6}J}, \end{aligned} \quad (\text{E31})$$

All spins deviate from local- xy planes since $\theta_a \neq 0$. The TM of the stationary condition is

$$\mathbf{M}_{\perp}^{\text{SIA}} = \frac{\sqrt{2}}{4(2 + 3A/J)} \left(\frac{A}{J}\right) \left(\frac{B}{J}\right) \hat{e}_{11\bar{2}}. \quad (\text{E32})$$

This is consistent with the numerical results in Fig. S4.

We present some parts of results by rotating \mathbf{B} in the manuscript. We also try other cases in Fig S5. When $\mathbf{B} \parallel [100]$, M_{\perp} vanishes for all α because of the twofold rotation symmetry. When $\mathbf{B} \parallel [101]$, M_{\perp} is finite only for

$\alpha = \pi/6 + n\pi$ and $\pi/2 + n\pi$. When $\mathbf{B} \parallel [110]$, M_{\perp} is finite only for $\alpha = \pi/6 + n\pi$ and $5\pi/6 + n\pi$. When $\mathbf{B} \parallel [112]$, M_{\perp} is finite only for $\alpha = \pi/6 + n\pi/3$.

3. Single-ion anisotropy ($A < 0$)

Let us consider Eq. E7 again, but $A < 0$. Then, since \mathbf{n}_a is an easy axis, the spins point to the easy axis. In pyrochlore lattice, the ground state of $H_J + H_{\text{SIA}}$ is an A_2 -order. The ground state manifold is now discretely degenerate, so the TM usually emerges when the symmetry admits.

When \mathbf{B} is applied to A_2 -order, each spin is confined in the plane spanned by its easy axis and \mathbf{B} . Let us try $\mathbf{B} \parallel [001]$ first, where the twofold rotation symmetry makes the TM vanishes. A_2 -order can be represented by Eq. E19, but the local axes are

$$\begin{aligned} \hat{x}_1 &= [\bar{1}\bar{1}2], \hat{x}_2 = [1\bar{1}2], \hat{x}_3 = [\bar{1}12], \hat{x}_4 = [112], \\ \hat{y}_1 &= [111], \hat{y}_2 = [1\bar{1}\bar{1}], \hat{y}_3 = [\bar{1}1\bar{1}], \hat{y}_4 = [\bar{1}\bar{1}1], \\ \hat{z}_1 &= [\bar{1}10], \hat{z}_2 = [110], \hat{z}_3 = [\bar{1}\bar{1}0], \hat{z}_4 = [1\bar{1}0]. \end{aligned} \quad (\text{E33})$$

Note that $x_a y_a$ -plane is spanned by A_2 -order and \mathbf{B} . Without \mathbf{B} , $\theta_a = \phi_a = 0$ for all a . The stationary condition can be found by Eq. E30 up to the second order of \mathbf{B} .

$$\begin{aligned} \theta_a = 0, \phi_1 = \phi_4 &= -\sqrt{\frac{3}{2}} \frac{B}{4J + 3A} + \frac{3}{2\sqrt{2}} \frac{B^2}{(4J + 3A)^2}, \\ \phi_2 = \phi_3 &= -\sqrt{\frac{3}{2}} \frac{B}{4J + 3A} - \frac{3}{2\sqrt{2}} \frac{B^2}{(4J + 3A)^2}. \end{aligned} \quad (\text{E34})$$

Note that for any order of B , $\theta_a = 0$. The spins are confined within local $x_a y_a$ -plane. The magnetization is $\mathbf{M} = \frac{\mathbf{B}}{4J + 3A}$.

This is different from the energy minimum condition. By adding some constant to Eq. E7, we have

$$\begin{aligned} H &= -\frac{4}{3}A \left[\sum_{r=1}^3 (\sqrt{2}M_r - \sum_a \mathbf{S}_a \cdot \mathbf{P}_a^r)^2 \right. \\ &\quad + 3 \left(\left(\sum_a \mathbf{S}_a \cdot \hat{x}_a \right)^2 + \left(\sum_a \mathbf{S}_a \cdot \hat{y}_a \right)^2 \right. \\ &\quad \left. \left. + \sum_{r=1}^3 \left(\sum_a \mathbf{S}_a \cdot \mathbf{T}_a^r \right)^2 \right) \right] + 8J \left(\mathbf{M} - \frac{\mathbf{B}}{4J} \right)^2, \end{aligned} \quad (\text{E35})$$

where \hat{x}_a and \hat{y}_a are defined in Eq. E11,

$$\begin{aligned} \mathbf{P}_1^1 &= [011], \mathbf{P}_2^1 = [0\bar{1}\bar{1}], \mathbf{P}_3^1 = [0\bar{1}1], \mathbf{P}_4^1 = [01\bar{1}], \\ \mathbf{P}_1^2 &= [101], \mathbf{P}_2^2 = [\bar{1}01], \mathbf{P}_3^2 = [\bar{1}0\bar{1}], \mathbf{P}_4^2 = [10\bar{1}], \\ \mathbf{P}_1^3 &= [110], \mathbf{P}_2^3 = [\bar{1}10], \mathbf{P}_3^3 = [1\bar{1}0], \mathbf{P}_4^3 = [\bar{1}\bar{1}0], \end{aligned} \quad (\text{E36})$$

and

$$\begin{aligned} \mathbf{T}_1^1 &= [01\bar{1}], \mathbf{T}_2^1 = [0\bar{1}1], \mathbf{T}_3^1 = [0\bar{1}\bar{1}], \mathbf{T}_4^1 = [011], \\ \mathbf{T}_1^2 &= [\bar{1}01], \mathbf{T}_2^2 = [101], \mathbf{T}_3^2 = [10\bar{1}], \mathbf{T}_4^2 = [\bar{1}0\bar{1}], \\ \mathbf{T}_1^3 &= [1\bar{1}0], \mathbf{T}_2^3 = [\bar{1}\bar{1}0], \mathbf{T}_3^3 = [110], \mathbf{T}_4^3 = [\bar{1}10]. \end{aligned} \quad (\text{E37})$$

Note that $\mathbf{M} = (M_1, M_2, M_3) = (M_x, M_y, M_z)$. \mathbf{P}_a^r and \mathbf{T}_a^r is related to T_1 and T_2 -octupole, respectively. Considering that the constants are positive, the energy minimum conditions are

$$\begin{aligned} \mathbf{M} &= \frac{\mathbf{B}}{4J}, \\ \sum_a \mathbf{S}_a \cdot \hat{x}_a &= 0, \\ \sum_a \mathbf{S}_a \cdot \hat{y}_a &= 0, \\ \sum_a \mathbf{S}_a \cdot \mathbf{T}_a^r &= 0 \quad (r = 1, 2, 3), \\ \sum_a \mathbf{S}_a \cdot \mathbf{P}_a^r &= \sqrt{2}M_r \quad (r = 1, 2, 3). \end{aligned} \quad (\text{E38})$$

The magnetization of the energy minimum condition is $\mathbf{M} = \mathbf{B}/4J$ which is different from stationary condition. This is because the stationary condition satisfying the energy minimum conditions generally does not exist since we have a total of 8 variables (θ_a, ϕ_a) and a total of 11 equations.

Let us try $\mathbf{B} \parallel [101]$, where the symmetries admits the TM. A_2 -order can be represented by Eq. E19, but the local axes are

$$\begin{aligned} \hat{x}_1 &= [\bar{1}2\bar{1}], \hat{x}_2 = [101], \hat{x}_3 = [121], \hat{x}_4 = [101], \\ \hat{y}_1 &= [111], \hat{y}_2 = [1\bar{1}\bar{1}], \hat{y}_3 = [\bar{1}1\bar{1}], \hat{y}_4 = [\bar{1}\bar{1}1], \\ \hat{z}_1 &= [\bar{1}01], \hat{z}_2 = [12\bar{1}], \hat{z}_3 = [\bar{1}01], \hat{z}_4 = [1\bar{2}\bar{1}]. \end{aligned} \quad (\text{E39})$$

Note that local- $x_a y_a$ plane is again spanned by A_2 -order and \mathbf{B} . Without \mathbf{B} , $\theta_a = \phi_a = 0$. The stationary condition is obtained by Eq. E30. Up to the second order of B ,

$$\begin{aligned} \theta_1 &= \theta_3 = 0, \theta_2 = -\theta_4 = \frac{9JB^2}{2\sqrt{2}(3A+4J)^3}, \\ \phi_1 &= -\frac{\sqrt{3}B}{2(3A+4J)} + \frac{3\sqrt{2}(3A+J)B^2}{4(3A+4J)^3}, \\ \phi_2 &= \phi_4 = -\frac{3B}{(3A+4J)}, \\ \phi_3 &= -\frac{\sqrt{3}B}{2(3A+4J)} - \frac{3\sqrt{2}(3A+J)B^2}{4(3A+4J)^3}, \end{aligned} \quad (\text{E40})$$

The TM is given by

$$\mathbf{M}_{\perp}^{SIA, A_2} = \frac{9\sqrt{3}}{8(3A/J+4)^3} \left(\frac{A}{J}\right) \left(\frac{B^2}{J^2}\right) \hat{y}. \quad (\text{E41})$$

We also find TM under \mathbf{B} in an arbitrary direction. In Fig. S6a, we present the change of TM under rotating \mathbf{B} from $[312]$ to $[101]$, and to $[\bar{5}23]$ in sequence. The TM arises for every direction.

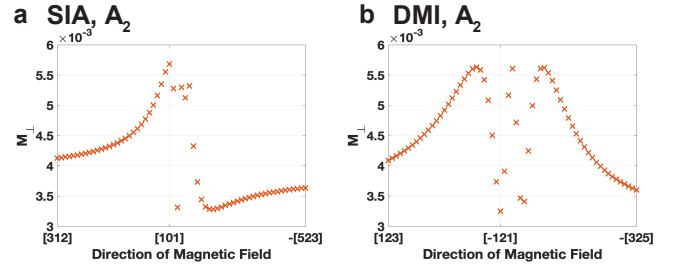


FIG. S6. The TM M_{\perp} for A_2 -order, (a) with SIA under \mathbf{B} changing from $[312]$ to $[101]$ to $[\bar{5}23]$, and (b) with DMI under \mathbf{B} changing from $[123]$ to $[\bar{1}21]$ to $[\bar{3}25]$.

4. Dzyaloshinskii-Moriya interaction ($D > 0$)

Next, let us consider DMI ($D > 0$) and A_2 -order.

$$\begin{aligned} H &= H_J + H_{DMI} + H_B \\ &= J \sum_{\langle ab \rangle} \mathbf{S}_a \cdot \mathbf{S}_b + D \sum_{\langle ab \rangle} \hat{\mathbf{D}}_{ab} \cdot (\mathbf{S}_a \times \mathbf{S}_b) - \mathbf{B} \cdot \sum_a \mathbf{S}_a. \end{aligned} \quad (\text{E42})$$

The role of DMI is to confine two spins in the plane perpendicular to the DM vector \mathbf{D}_{ij} because the energy is minimized when $\mathbf{S}_i \times \mathbf{S}_j$ is anti-parallel to \mathbf{D}_{ij} . When we consider the unit cell of pyrochlore lattice, each spin prefers to be perpendicular to the surrounding six DM vectors. The perpendicular direction to the DM vectors is the local- z axis of \mathbf{S}_i . Hence, DMI confines \mathbf{S}_i to its local- z axis, and the ground state is A_2 -octupole, as same as the previous section. Again, the ground state manifold is now discretely degenerate, and the TM can arise when the symmetry admits.

When \mathbf{B} is applied, it is natural that each spin is confined in the plane spanned by its local- z axis and \mathbf{B} . We try other directions from the previous section since the result is similar. When $\mathbf{B} \parallel [100]$, the TM is canceled by twofold rotation symmetry. A_2 -order can be represented by Eq. E19, but the local axes are changed by

$$\begin{aligned} \hat{x}_1 &= [2\bar{1}\bar{1}], \hat{x}_2 = [211], \hat{x}_3 = [21\bar{1}], \hat{x}_4 = [2\bar{1}1], \\ \hat{y}_1 &= [111], \hat{y}_2 = [1\bar{1}\bar{1}], \hat{y}_3 = [\bar{1}1\bar{1}], \hat{y}_4 = [\bar{1}\bar{1}1], \\ \hat{z}_1 &= [0\bar{1}1], \hat{z}_2 = [01\bar{1}], \hat{z}_3 = [011], \hat{z}_4 = [0\bar{1}\bar{1}]. \end{aligned} \quad (\text{E43})$$

Note that $x_a y_a$ -plane is spanned by A_2 -order and \mathbf{B} . Without \mathbf{B} , $\theta_a = \phi_a = 0$ for all a . The stationary condition under \mathbf{B} can be found by Eq. E30 up to the second order of B .

$$\begin{aligned} \theta_a &= 0, \\ \phi_1 &= \phi_2 = -\sqrt{\frac{3}{2}} \frac{B}{7D+4J} + \frac{3B^2}{2\sqrt{2}(7D+4J)^2}, \\ \phi_3 &= \phi_4 = -\sqrt{\frac{3}{2}} \frac{B}{7D+4J} - \frac{3B^2}{2\sqrt{2}(7D+4J)^2}. \end{aligned} \quad (\text{E44})$$

Note that for any order of B , $\theta_a = 0$. Hence, the spins are confined within $x_a y_a$ -plane. The magnetization is just $\mathbf{M} = \frac{\mathbf{B}}{7D+4J}$.

Please note that this is different from the energy minimum condition of DMI. By adding some constant to Equation E42, we have

$$\begin{aligned}
H = & 8(J+D)\left(\mathbf{M} - \frac{\mathbf{B}}{4(J+D)}\right)^2 + 4D[\\
& 3\left(\sum_a \mathbf{S}_a \cdot \hat{x}_a/4\right)^2 + 3\left(\sum_a \mathbf{S}_a \cdot \hat{y}_a/4\right)^2 \\
& + 3\sum_{r=1}^3 \left(\sum_a \mathbf{S}_a \cdot \mathbf{P}_a^r/4\right)^2 \\
& + \sum_{r=1}^3 \left(\sum_a \mathbf{S}_a \cdot \mathbf{T}_a^r/4\right)^2], \quad (\text{E45})
\end{aligned}$$

where \hat{x}_a and \hat{y}_a are defined in Eq. E11, and \mathbf{P}_a^r and \mathbf{T}_a^r are defined in Eq. E36 and E37. Considering that all coefficients are positive, the energy minimum condition is given by

$$\begin{aligned}
\mathbf{M} &= \frac{\mathbf{B}}{4(J+D)}, \\
\sum_a \mathbf{S}_a \cdot x_a &= 0, \\
\sum_a \mathbf{S}_a \cdot y_a &= 0, \\
\sum_a \mathbf{S}_a \cdot \mathbf{P}_a^r &= 0 \quad (r = 1, 2, 3), \\
\sum_a \mathbf{S}_a \cdot \mathbf{T}_a^r &= 0 \quad (r = 1, 2, 3), \quad (\text{E46})
\end{aligned}$$

Here, the magnetization of energy minimum condition is $\mathbf{M} = \frac{\mathbf{B}}{4(J+D)}$ which is different from stationary condition. This is because the stationary condition satisfying the energy minimum conditions generally does not exist for discretely degenerate case, as we have a total of 8 variables (θ_a, ϕ_a) and a total of 11 equations.

For $\mathbf{B} \parallel [110]$, on the other hand, the TM is admitted by symmetry breaking. A_2 -order can be represented again by Eq. E19, but the local axes are now

$$\begin{aligned}
\hat{x}_1 &= \hat{x}_4 = [1\bar{1}0], \hat{x}_2 = [\bar{1}1\bar{2}], \hat{x}_3 = [\bar{1}12] \\
\hat{y}_1 &= [111], \hat{y}_2 = [1\bar{1}\bar{1}], \hat{y}_3 = [\bar{1}1\bar{1}], \hat{y}_4 = [\bar{1}\bar{1}1], \\
\hat{z}_1 &= [11\bar{2}], \hat{z}_2 = \hat{z}_3 = [110], \hat{z}_4 = [112]. \quad (\text{E47})
\end{aligned}$$

Note that $x_a y_a$ -plane is spanned by A_2 -order and \mathbf{B} . Without \mathbf{B} , $\theta_a = 0$ and $\phi_a = 0$. The stationary condition under B can be found by Eq. E30. Up to the second order of B

$$\begin{aligned}
\theta_1 &= \theta_4 = 0, \theta_2 = -\theta_3 = \frac{9(D-2J)}{4\sqrt{2}(7D+4J)^3} B^2, \\
\phi_1 &= -\frac{\sqrt{3}}{2(7D+4J)} B + 3\frac{(17D+2J)}{4\sqrt{2}(7D+4J)^3} B^2, \\
\phi_2 &= \phi_3 = -\frac{3}{2(7D+4J)} B, \\
\phi_4 &= -\frac{\sqrt{3}}{2(7D+4J)} B - 3\frac{(17D+2J)}{4\sqrt{2}(7D+4J)^3} B^2. \quad (\text{E48})
\end{aligned}$$

Since $\theta_{2,3} \neq 0$, \mathbf{S}_2 and \mathbf{S}_3 deviate from the plane spanned by \mathbf{B} and \hat{y}_a . The TM in the stationary condition is

$$\mathbf{M}_\perp^{DM} = \frac{27\sqrt{3}}{8(4+7D/J)^3} \left(\frac{D}{J}\right) \left(\frac{B^2}{J^2}\right) \hat{z}. \quad (\text{E49})$$

We also find TM under \mathbf{B} in an arbitrary direction. In Fig. S6b, we present the change of TM under rotating \mathbf{B} from $[123]$ to $[\bar{1}21]$, and to $[\bar{3}2\bar{5}]$ in sequence. The TM arises for every direction.

5. Dzyloshinskii-Moriya Interaction ($D < 0$)

Next, let us consider DMI ($D < 0$). A_2 -order is not ground state anymore because A_2 -order gains energy. We can acquire the energy minimum condition by adding some constants to Eq. E42.

$$\begin{aligned}
H = & -12D\left(\sum_a \mathbf{S}_a \cdot \hat{v}_a/4\right)^2 - 8D\sum_{r=1}^3 \left[\left(\sum_a \mathbf{S}_a \cdot \mathbf{T}_a^r/4\right)^2\right] \\
& + 8(J-D/2)\left(\mathbf{M} - \frac{\mathbf{B}}{4(J-D/2)}\right)^2, \quad (\text{E50})
\end{aligned}$$

where

$$\hat{v}_1 = [111], \hat{v}_2 = [1\bar{1}\bar{1}], \hat{v}_3 = [\bar{1}1\bar{1}], \hat{v}_4 = [\bar{1}\bar{1}1], \quad (\text{E51})$$

and \mathbf{T}_a^r is defined in Eq. E37. Since $D < 0$, all coefficients are positive, so the energy minimum conditions are

$$\begin{aligned}
\sum_a \mathbf{S}_a \cdot \hat{v}_a &= 0, \\
\sum_a \mathbf{S}_a \cdot \mathbf{T}_a^r &= 0 \quad (r = 1, 2, 3), \\
\mathbf{M} &= \frac{\mathbf{B}}{4(J-D/2)}. \quad (\text{E52})
\end{aligned}$$

If $\mathbf{B} = 0$, the energy minimum spin configuration can be found by setting

$$\begin{aligned}
\mathbf{S}_a &= \cos \phi_a \sin \theta_a \hat{x}_a \\
&+ \sin \phi_a \sin \theta_a \hat{y}_a + \cos \theta_a \hat{z}_a, \quad (\text{E53})
\end{aligned}$$

whose local axes are defined in Eq. E11. Then, the conditions give rise to $\theta_a = \pi/2$ and $\phi_1 = \phi_2 = \phi_3 = \phi_4 = \alpha$, which corresponds to $E(\alpha)$ -order. Furthermore, we find that $E + T_1$ -orders are also the energy minimum spin configurations, which is represented by

$$\mathbf{S}_a = \cos \beta \hat{x}_a + \sin \beta \hat{y}_a, \quad (\text{E54})$$

where the local axes are

$$\begin{aligned}
\hat{x}_1 &= [011], \hat{x}_2 = [0\bar{1}\bar{1}], \hat{x}_3 = [0\bar{1}1], \hat{x}_4 = [01\bar{1}], \\
\hat{y}_1 &= [0\bar{1}1], \hat{y}_2 = [01\bar{1}], \hat{y}_3 = [0\bar{1}\bar{1}], \hat{y}_4 = [011], \\
\hat{z}_a &= [100], \quad (\text{E55})
\end{aligned}$$

or

$$\begin{aligned}\hat{x}_1 &= [101], \hat{x}_2 = [\bar{1}01], \hat{x}_3 = [\bar{1}0\bar{1}], \hat{x}_4 = [10\bar{1}], \\ \hat{y}_1 &= [10\bar{1}], \hat{y}_2 = [101], \hat{y}_3 = [\bar{1}01], \hat{y}_4 = [\bar{1}0\bar{1}], \\ \hat{z}_a &= [010],\end{aligned}\quad (\text{E56})$$

or

$$\begin{aligned}\hat{x}_1 &= [110], \hat{x}_2 = [\bar{1}10], \hat{x}_3 = [1\bar{1}0], \hat{x}_4 = [\bar{1}\bar{1}0], \\ \hat{y}_1 &= [\bar{1}\bar{1}0], \hat{y}_2 = [110], \hat{y}_3 = [\bar{1}\bar{1}0], \hat{y}_4 = [110], \\ \hat{z}_a &= [00\bar{1}].\end{aligned}\quad (\text{E57})$$

Note that \hat{x}_a are the spin directions in T_{1x} , T_{1y} , and T_{1z} -orders, \hat{y}_a are that in $E(-\pi/3)$, $E(\pi/3)$, and E_2 -orders in sequence. The energy of $E + T_1$ -order is the same as $E(\alpha)$ -order, because $\mathbf{S}_a \times \mathbf{S}_b$ remain invariant while β varies. Note that for each $E + T_1$ -order, all spins are in the same plane. For example, all spins in $E_2 + T_{1z}$ -order are in xy -plane, those in $E(\pi/3) + T_{1y}$ -order are in xz -plane, and those in $E(-\pi/3) + T_{1x}$ -order are in yz -plane.

Since the ground state is continuously degenerate, TM usually vanishes when \mathbf{B} is applied. Let us choose a general $E(\alpha)$ -order as a ground state for convenience. For small magnetic field \mathbf{B} , the spins are described by

$$\begin{aligned}\mathbf{S}_a &= \cos(\alpha + \phi_a) \cos(\theta_a) \hat{x}_a \\ &+ \sin(\alpha + \phi_a) \cos(\theta_a) \hat{y}_a - \sin \theta_a \hat{z}_a\end{aligned}\quad (\text{E58})$$

where the local axes are defined in Eq. E11, and (θ_a, ϕ_a) is the angle deviation by \mathbf{B} . Up to the first order of angles, the spins are expanded as

$$\begin{aligned}\mathbf{S}_a &= (\cos \alpha - \phi_a \sin \alpha) \hat{x}_a \\ &+ (\phi_a \cos \alpha + \sin \alpha) \hat{y}_a - \theta_a \hat{z}_a.\end{aligned}\quad (\text{E59})$$

We put the expansion in Eq. E52,

$$\begin{aligned}\sum_a \mathbf{S}_a \cdot \hat{v}_a &= -\frac{1}{4} \sum_a \theta_a = 0, \\ \sum_a \mathbf{S}_a \cdot \mathbf{T}_a^1 &= \frac{1}{8} (\phi_1 + \phi_2 - \phi_3 - \phi_4) \\ &\times (\sqrt{3} \cos \alpha + \sin \alpha) = 0, \\ \sum_a \mathbf{S}_a \cdot \mathbf{T}_a^2 &= -\frac{1}{8} (\phi_1 - \phi_2 + \phi_3 - \phi_4) \\ &\times (\sqrt{3} \cos \alpha - \sin \alpha) = 0, \\ \sum_a \mathbf{S}_a \cdot \mathbf{T}_a^3 &= \frac{1}{4} (-\phi_1 + \phi_2 + \phi_3 - \phi_4) \sin \alpha = 0,\end{aligned}$$

and

$$\begin{aligned}\mathbf{M} &= \left[\frac{1}{24} (-\phi_1 - \phi_2 + \phi_3 + \phi_4) (\sqrt{6} \cos \alpha - 3\sqrt{2} \sin \alpha) \right. \\ &+ \frac{1}{4\sqrt{3}} (-\theta_1 - \theta_2 + \theta_3 + \theta_4), \\ &\frac{1}{24} (\phi_1 - \phi_2 + \phi_3 - \phi_4) (\sqrt{6} \cos \alpha + 3\sqrt{2} \sin \alpha) \\ &+ \frac{1}{4\sqrt{3}} (-\theta_1 + \theta_2 - \theta_3 + \theta_4), \\ &- \frac{\sqrt{2}}{4\sqrt{3}} (\phi_1 - \phi_2 - \phi_3 + \phi_4) \cos \alpha \\ &\left. + \frac{1}{4\sqrt{3}} (-\theta_1 + \theta_2 + \theta_3 - \theta_4) \right] = \frac{\mathbf{B}}{4(J - D/2)}.\end{aligned}\quad (\text{E60})$$

We find the solution by expanding (θ_a, ϕ_a) as a series of B and take terms only up to B . When $B = |\mathbf{B}|$,

$$\theta_a = -3\hat{z}_a \cdot \frac{\mathbf{B}}{4(J - D/2)}, \phi_a = q \frac{B}{4(J - D/2)}, \quad (\text{E61})$$

where q is an arbitrary constant, and \hat{z}_a is in Eq. E11. Accordingly, we acquire the magnetization,

$$\mathbf{M} = \frac{\mathbf{B}}{4(J - D/2)}.\quad (\text{E62})$$

Please note that when we try Eq. E30 to find the stationary condition, we have the same result in Eqs. E61-E62 for the general $E(\alpha)$ -order. This is different from SIA $A > 0$ case, where all spins are confined to the local- xy planes.

We also analytically find that the stationary condition also gives $\mathbf{M} = \frac{\mathbf{B}}{(J - D/2)}$ for arbitrary $E(\alpha)$ -order. The TM vanishes for any α . This is consistent with numerical calculations in a generic $E(\alpha)$ -order, as shown in Figs. S4c,e,g. It is still valid that the TM generally vanishes in continuous degenerate ground states.

We perform the same procedure to $E + T_1$ -orders. For $E_2 + T_{1z}(\beta)$ -order, for example, the spins under \mathbf{B} are described by

$$\begin{aligned}\mathbf{S}_a &= \cos \theta_a \cos(\beta + \phi_a) \hat{x}_a + \cos \theta_a \sin(\beta + \phi_a) \hat{y}_a \\ &+ \sin \theta_a \hat{z}_a,\end{aligned}\quad (\text{E63})$$

where

$$\begin{aligned}\hat{x}_1 &= [1\bar{1}0], \hat{x}_2 = [110], \hat{x}_3 = [\bar{1}\bar{1}0], \hat{x}_4 = [\bar{1}10], \\ \hat{y}_1 &= [110], \hat{y}_2 = [\bar{1}10], \hat{y}_3 = [1\bar{1}0], \hat{y}_4 = [\bar{1}\bar{1}0], \\ \hat{z}_a &= [00\bar{1}].\end{aligned}\quad (\text{E64})$$

The expansion gives rise to

$$\begin{aligned}\mathbf{S}_a &= (\cos \beta - \sin \beta \phi_a) \hat{x}_a + (\sin \beta + \cos \beta \phi_a) \hat{y}_a \\ &+ \theta_a \hat{z}_a\end{aligned}\quad (\text{E65})$$

The energy minimum condition in Eq. E52 gives

$$\begin{aligned}
\sum_a \mathbf{S}_a \cdot \hat{v}_a &= \frac{1}{4\sqrt{3}}(\theta_1 - \theta_2 - \theta_3 + \theta_4 \\
&+ \sqrt{2} \cos \beta (\phi_1 - \phi_2 - \phi_3 + \phi_4)) = 0, \\
\sum_a \mathbf{S}_a \cdot \mathbf{T}_a^1 &= \frac{1}{4\sqrt{2}}((\phi_1 - \phi_2 + \phi_3 - \phi_4) \cos \beta \\
&+ (-\phi_1 - \phi_2 + \phi_3 + \phi_4) \sin \beta) = 0, \\
\sum_a \mathbf{S}_a \cdot \mathbf{T}_a^2 &= \frac{1}{4\sqrt{2}}((\phi_1 + \phi_2 - \phi_3 - \phi_4) \cos \beta \\
&+ (\phi_1 - \phi_2 + \phi_3 - \phi_4) \sin \beta) = 0, \\
\sum_a \mathbf{S}_a \cdot \mathbf{T}_a^3 &= \frac{1}{4}(\sum_a \theta_a) = 0,
\end{aligned}$$

and

$$\begin{aligned}
\mathbf{M} &= \left[\frac{1}{8}(\sqrt{2}(\theta_1 + \theta_2 - \theta_3 - \theta_4) + (\phi_1 - \phi_2 + \phi_3 - \phi_4) \cos \beta \right. \\
&+ (\phi_1 + \phi_2 - \phi_3 - \phi_4) \sin \beta), \\
&\frac{1}{8}(\sqrt{2}(\theta_1 + \theta_2 - \theta_3 - \theta_4) + (-\phi_1 - \phi_2 + \phi_3 + \phi_4) \cos \beta \\
&+ (\phi_1 - \phi_2 + \phi_3 - \phi_4) \sin \beta), \\
&\left. - \frac{1}{4}(\phi_1 - \phi_2 - \phi_3 + \phi_4) \sin \beta \right] = \frac{\mathbf{B}}{4(J - D/2)}. \quad (\text{E66})
\end{aligned}$$

When $\mathbf{B} = B(b_x, b_y, b_z)$ and $B = |\mathbf{B}|$, the solution of the system of equations is

$$\begin{aligned}
\theta_1 &= \frac{B}{4(J - D/2)}(b_z + (b_x + b_y) \cos(2\beta) \\
&+ (-b_x + b_y) \sin(2\beta)), \\
\theta_2 &= \frac{B}{4(J - D/2)}(b_z + (-b_x + b_y) \cos(2\beta) \\
&+ (-b_x - b_y) \sin(2\beta)), \\
\theta_3 &= \frac{B}{4(J - D/2)}(b_z + (b_x - b_y) \cos(2\beta) \\
&+ (b_x + b_y) \sin(2\beta)), \\
\theta_4 &= \frac{B}{4(J - D/2)}(b_z + (-b_x - b_y) \cos(2\beta) \\
&+ (b_x - b_y) \sin(2\beta)), \\
\phi_2 &= \phi_1 - \frac{2\sqrt{2}B}{4(J - D/2)}(b_x \cos \beta + b_y \sin \beta), \\
\phi_3 &= \phi_1 + \frac{2\sqrt{2}B}{4(J - D/2)}(-b_y \cos \beta + b_x \sin \beta), \\
\phi_4 &= \phi_1 + \frac{2\sqrt{2}B}{4(J - D/2)}(-(b_x + b_y) \cos \beta \\
&+ (b_x - b_y) \sin \beta), \quad (\text{E67})
\end{aligned}$$

The TM vanishes for arbitrary β as well.

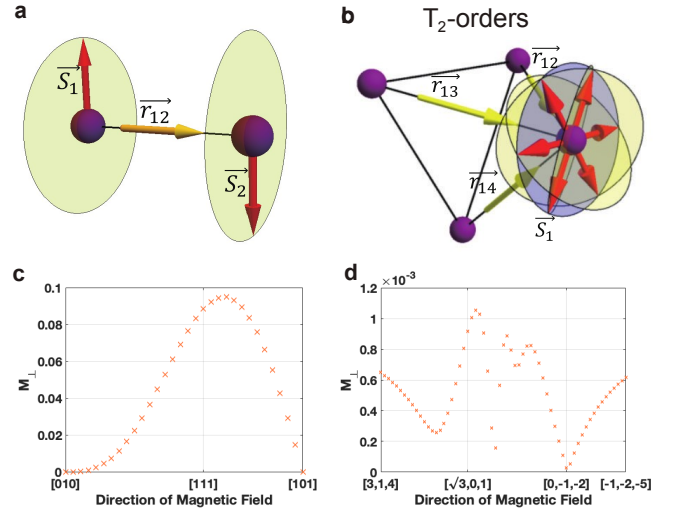


FIG. S7. (a) The role of DI. The spins \mathbf{S}_1 and \mathbf{S}_2 that are apart by \mathbf{r}_{12} are confined in the plane perpendicular to \mathbf{r}_{12} . (a-b) The yellow arrows are the displacement vectors, the red arrows are the spins, the yellow planes are the planes perpendicular to displacement vectors. (b) \mathbf{S}_1 is surrounded by \mathbf{r}_{12} , \mathbf{r}_{13} , \mathbf{r}_{14} . However, the intersecting line of planes perpendicular to \mathbf{r}_{12} , \mathbf{r}_{13} , and \mathbf{r}_{14} (yellow planes) is absent. Instead, \mathbf{S}_1 is at the intersection of one of such three planes and the blue plane perpendicular to the $\mathbf{r}_{12} + \mathbf{r}_{13} + \mathbf{r}_{14} \propto [111]$. Accordingly, the ground state of pyrochlore lattice with DI is three \mathbf{T}_2 -orders up to time-reversal. We choose T_{2y} -order as a ground state. (c) Changing \mathbf{B} from $[010]$ to $[111]$ and to $[101]$, M_{\perp} for T_{2y} -order are plotted. Only at $\mathbf{B} \parallel [010]$ or $[101]$, M_{\perp} vanishes. (d) Changing \mathbf{B} from $[314]$ to $[\sqrt{3}01]$, to $[01\bar{2}]$, and to $[\bar{1}\bar{2}5]$ in sequence, M_{\perp} are plotted.

6. Dipolar interaction

Lastly, let us discuss DI ($J_{DI} > 0$) and T_{2y} -order.

$$\begin{aligned}
H &= H_J + H_{DI} + H_B, \\
&= J \sum_{\langle ab \rangle} \mathbf{S}_a \cdot \mathbf{S}_b + J_{DI} \sum_{\langle ab \rangle} [\mathbf{S}_a \cdot \mathbf{S}_b - 3(\mathbf{S}_a \cdot \mathbf{r}_{ab})(\mathbf{S}_b \cdot \mathbf{r}_{ab})] \\
&\quad - \mathbf{B} \cdot \sum_a \mathbf{S}_a. \quad (\text{E68})
\end{aligned}$$

To get an insight for DI, let us first consider a 2-spin system with \mathbf{S}_1 and \mathbf{S}_2 apart by \mathbf{r}_{12} interacting with $H = H_J + H_{DI}$, as shown in Fig. S7a. There is a competition between H_J and H_{DI} , since H_J prefers the antiferromagnet and H_{DI} prefers the ferromagnet along \mathbf{r}_{12} . However, since J is much stronger than J_{DI} , the ground state is an antiferromagnet. Instead, H_{DI} makes two spins confined in the plane perpendicular to \mathbf{r}_{ij} . Two spins can freely rotate within the plane, but they are at the opposite direction to each other.

When we have the unit cell of pyrochlore lattice, there are three displacement vectors for each spin. Note that we consider only the nearest neighbor DI for convenience.²⁶ For example, \mathbf{S}_1 is surrounded by $\mathbf{r}_{12} = [011]/\sqrt{2}$, $\mathbf{r}_{13} = [101]/\sqrt{2}$, and $\mathbf{r}_{14} = [110]/\sqrt{2}$ (see Fig. S7b). The planes perpendicular to \mathbf{r}_{12} , \mathbf{r}_{13} , and \mathbf{r}_{14} have no intersecting lines. Instead, the energy minimum is on one of three planes and

perpendicular to $\mathbf{r}_{12} + \mathbf{r}_{13} + \mathbf{r}_{14} \propto [111]$, which is indicated by red arrows in Fig. S7c. This argument are the same for the other spins. We have total 6 minimums for each spin as follows.

$$\begin{aligned}\mathbf{S}_1 &: \pm[01\bar{1}], \pm[\bar{1}01], \pm[1\bar{1}0], \\ \mathbf{S}_2 &: \pm[0\bar{1}1], \pm[101], \pm[\bar{1}10], \\ \mathbf{S}_3 &: \pm[0\bar{1}\bar{1}], \pm[10\bar{1}], \pm[110], \\ \mathbf{S}_4 &: \pm[011], \pm[\bar{1}0\bar{1}], \pm[\bar{1}10].\end{aligned}\quad (\text{E69})$$

When we choose one of 6 minimums of \mathbf{S}_1 , the other spins are automatically chosen. For example, let us choose $\mathbf{S}_1 \parallel [\bar{1}01]$. Since $H_J + H_{DI}$ prefers two spins pointing opposite directions, $\mathbf{S}_3 \parallel [10\bar{1}]$. The energy from interacting $\mathbf{S}_1, \mathbf{S}_3$ and $\mathbf{S}_2, \mathbf{S}_4$ is minimized when $\mathbf{S}_2 \parallel [101]$, $\mathbf{S}_4 \parallel [\bar{1}0\bar{1}]$ because $\mathbf{S}_2, \mathbf{S}_4 \perp \mathbf{S}_1, \mathbf{S}_3$. Note that \mathbf{S}_2 and \mathbf{S}_4 are pointing opposite to each other. This spin configuration corresponds to T_{2y} -order. Other choices give T_{2x}, T_{2z} -orders, similarly. Unlike two site case, where ferromagnetic and antiferromagnetic orders compete, $T_{2i}(i = x, y, z)$ -order is always the ground state for any $J_{DI} > 0$ in the unit cell of pyrochlore lattice. The ground state is now discretely degenerate, and the TM usually arises when the symmetry admits.

Let us find the ground state under \mathbf{B} . When $\mathbf{B} \parallel [010]$, the TM vanishes by twofold rotation symmetry. \mathbf{S}_a is represented by Eq. E19, whose local axes are

$$\begin{aligned}\hat{x}_1 &= [121], \hat{x}_2 = [\bar{1}21], \hat{x}_3 = [\bar{1}2\bar{1}], \hat{x}_4 = [12\bar{1}], \\ \hat{y}_1 &= [\bar{1}01], \hat{y}_2 = [101], \hat{y}_3 = [10\bar{1}], \hat{y}_4 = [\bar{1}0\bar{1}], \\ \hat{z}_1 &= [1\bar{1}1], \hat{z}_2 = [11\bar{1}], \hat{z}_3 = [\bar{1}\bar{1}\bar{1}], \hat{z}_4 = [\bar{1}11].\end{aligned}\quad (\text{E70})$$

When $\mathbf{B} = 0$, $\theta_a = \phi_a = 0$. The stationary condition under finite \mathbf{B} can be obtained by Eq. E30 up to third order of B ,

$$\theta_a = 0, \phi_a = -\frac{\sqrt{6}B}{2(4J + J_{DI})} - \frac{\sqrt{6}B^3}{8(4J + J_{DI})^3}. \quad (\text{E71})$$

As $\theta_a = 0$, all spins are confined in $x_a y_a$ -planes. Accordingly, the magnetization is $\mathbf{M} = \frac{\mathbf{B}}{4J + J_{DI}}$.

On the other hand, when $\mathbf{B} \parallel [111]$, the symmetry breaking admits the TM. \mathbf{S}_a is in Eq. E19, whose the local axes are

$$\begin{aligned}\hat{x}_1 &= [525], \hat{x}_2 = [\bar{1}21], \hat{x}_3 = [323], \hat{x}_4 = [111], \\ \hat{y}_1 &= [\bar{1}01], \hat{y}_2 = [101], \hat{y}_3 = [10\bar{1}], \hat{y}_4 = [\bar{1}0\bar{1}], \\ \hat{z}_1 &= [1\bar{5}1], \hat{z}_2 = [11\bar{1}], \hat{z}_3 = [\bar{1}3\bar{1}], \hat{z}_4 = [\bar{1}11].\end{aligned}\quad (\text{E72})$$

Again, $\theta_a, \phi_a = 0$ when $\mathbf{B} = 0$. With finite \mathbf{B} , from Eq. E30,

the stationary condition is obtained

$$\begin{aligned}\theta_1 &= \frac{16(8J + 17J_{DI})}{135(4J + J_{DI})^4} B^3, \\ \theta_2 &= \frac{4\sqrt{2}}{3\sqrt{3}(4J + J_{DI})^2} B^2 - \frac{4}{45(4J + J_{DI})^3} B^3, \\ \theta_3 &= \frac{8(4J - 5J_{DI})}{3\sqrt{33}(4J + J_{DI})^4} B^3, \\ \theta_4 &= \frac{-4\sqrt{2}}{3\sqrt{3}(4J + J_{DI})^2} B^2 - \frac{4}{45(4J + J_{DI})^3} B^3, \\ \phi_1 &= \frac{-4028J + 3793J_{DI}}{540\sqrt{2}(4J + J_{DI})^4} B^3, \\ \phi_2 &= \frac{2}{3\sqrt{3}(4J + J_{DI})^2} B^2 - \frac{71}{180\sqrt{2}(4J + J_{DI})^3} B^3, \\ \phi_3 &= \frac{268J + 8707J_{DI}}{180\sqrt{66}(4J + J_{DI})^4} B^3, \\ \phi_4 &= \frac{-2}{3\sqrt{3}(4J + J_{DI})^2} B^2 - \frac{71}{180\sqrt{2}(4J + J_{DI})^3} B^3.\end{aligned}\quad (\text{E73})$$

As $\theta_a \neq 0$, the spins are away from $x_a y_a$ -planes. Accordingly, the TM is

$$\mathbf{M}_\perp^{DI} = -\frac{4\sqrt{2}}{3(4 + J_{DI}/J)^4} \left(\frac{J_{DI}}{J}\right) \left(\frac{B^3}{J^3}\right) \hat{e}_{1\bar{2}1}. \quad (\text{E74})$$

We analytically calculate the TM by changing \mathbf{B} from $[010]$ to $[111]$ and to $[101]$ in sequence (see Fig. S7c). Also, we change \mathbf{B} in arbitrary directions shown in Fig. S7d. \mathbf{M}_\perp vanishes only at $[010]$ and $[101]$ but is finite otherwise. Note that considering the symmetry, the TM vanishes under $[010]$ and $[101]$, but is finite otherwise. We plot \mathbf{M}_\perp^{DI} in units of $J_{DI}/J = 0.1$, $B/J = 1$ in Figs. S7c-d.

Appendix F: Application to experiments

Here we apply our theory to the reported experimental results of TM.

1. CsMnBr₃

In CsMnBr₃, $\mathbf{M}_\perp \propto B$ was observed when \mathbf{B} is applied within xz -plane, unless \mathbf{B} is parallel to the x or z -axis.¹⁷ To numerically calculate \mathbf{M}_\perp , we consider the following spin model relevant to CsMnBr₃

$$\begin{aligned}H &= J \sum_{ij} \mathbf{S}_i \cdot \mathbf{S}_j + J' \sum_{ij} \mathbf{S}_i \cdot \mathbf{S}_j \\ &\quad + A \sum_i (S_i^z)^2 - \mathbf{B} \cdot \sum_i \mathbf{S}_i,\end{aligned}\quad (\text{F1})$$

where J (J') is the Heisenberg interaction between intra-layer (inter-layer) nearest neighbors, $A > 0$ is the single-ion

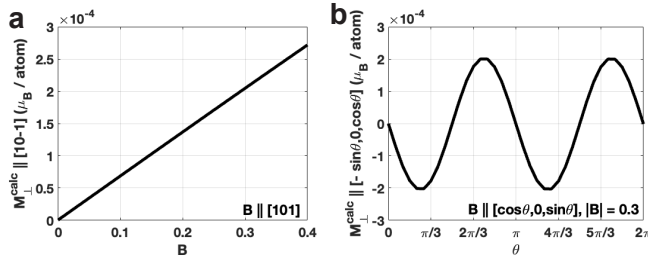


FIG. S8. Numerical calculations of \mathbf{M}_\perp using the spin Hamiltonian relevant to CsMnBr_3 . (a) $\mathbf{M}_\perp^{\text{calc}}$ when $\mathbf{B} \parallel [101]$ as a function of $|\mathbf{B}| = B$. (b) $\mathbf{M}_\perp^{\text{calc}}$ when $\mathbf{B} \parallel [\cos \theta, 0, \sin \theta]$ and $B = 0.3$, varying θ .

anisotropy.⁴³ Here \sum' (\sum'') is the summation over intra-layer (inter-layer) neighbors. The parameters are chosen as $J = 2.14$, $J' = 0.005$, $A = 0.0195$. The numerically obtained $\mathbf{M}_\perp^{\text{calc}}$ is shown in Figs. S8a-b. For $\mathbf{B} \parallel [101]$, we find $\mathbf{M}_\perp^{\text{calc}} \parallel [10\bar{1}] \propto B$ (see Fig. S8a) while for $\mathbf{B} \parallel [\cos \theta, 0, \sin \theta]$, we obtain $\mathbf{M}_\perp^{\text{calc}} = 0$ when $\mathbf{B} \parallel \hat{x}$ or \hat{z} (see Fig. S8b), which are compatible with the experimental results.

The above numerical results can be understood using the symmetry of CsMnBr_3 whose space group is 194 and magnetic space group is 189.225 ($P6_2'm'$). The 6 Mn atoms in the magnetic unit cell form a single spin cluster. The crystalline point group of the unit cell is D_{3h} , which is generated by rotations C_{3z} , C_{2x} , and horizontal mirror M_z .

We have total 18 degrees of freedom of spins in total. The system has 3 cluster dipoles, 7 octupoles, 6 dotriacontapoles, and 2 128-poles. Dipoles are decomposed into A'_2 and E'' , octupoles are decomposed into $A'_1, A'_2, A'_2, E',$ and E'' , dotriacontapoles are decomposed into 2 E' and E'' , and 128-poles are decomposed into A'_1 and A'_1 . The spin configuration of each CMM is shown in SI. The ground state is composed of A'_1 -128-pole, which we denote as A'_1 -order. (See Fig. S2.) The magnetic point group of A'_1 -order is just $D_{3h}(-6m2)$. When $\mathbf{B} \parallel z$, the magnetic point group is $\{I, 2C_3, M_z, 2M_zC_3\}$. On the other hand, when $\mathbf{B} \parallel x$, the magnetic point group is $\{I, M_x\}$. Hence, in both cases, \mathbf{M}_\perp vanishes.

When magnetic field is applied in xz -plane, the magnetic point group is $\{I\}$, but the symmetry inverting \mathbf{B} is $\{C_{2y}\}$. Using the argument in Sec. A, the sum of spin changes is

$$\begin{aligned}\Delta S_x(\mathbf{B}) &= -\Delta S_x(-\mathbf{B}), \\ \Delta S_y(\mathbf{B}) &= \Delta S_y(-\mathbf{B}), \\ \Delta S_z(\mathbf{B}) &= -\Delta S_z(-\mathbf{B}),\end{aligned}\quad (\text{F2})$$

Hence, when $\mathbf{B} \parallel [\cos \theta, 0, \sin \theta]$, $\mathbf{M}_\perp \parallel [-\sin \theta, 0, \cos \theta]$ is an odd function of \mathbf{B} . This is consistent with Figs. S8a-b.

2. $\text{Gd}_2\text{Ti}_2\text{O}_7$

$\text{Gd}_2\text{Ti}_2\text{O}_7$ is a pyrochlore material, where only Gd electrons have magnetism. Though the ground state of Gd^{3+} is $^8S_{7/2}$, the strong spin orbit coupling induces nonzero orbital

angular momentum and thus a strong single-ion anisotropy appears. It has a complicated phase diagram near 1 K; it is known to have a 4- k structure between 0.75 - 1.05 K,⁴⁴ and have a local-XY structure (E_2 -order) below 0.75 K.^{19,20} Below 0.75 K, it is reported that $\mathbf{M}_\perp = 0$ for $\mathbf{B} \parallel [001], [110]$ while $\mathbf{M}_\perp \neq 0$ for $\mathbf{B} \parallel [111], [112]$.¹⁸ The reported \mathbf{M}_\perp is consistent with our numerical calculation in Fig. S4. That is, at weak field, $\mathbf{M}_\perp = 0$, but at strong field \mathbf{M}_\perp becomes nonzero.

First, according to the last row of Table S1, \mathbf{M}_\perp vanishes $\mathbf{B} \parallel [001]$ or $[110]$, while \mathbf{M}_\perp appears for $\mathbf{B} \parallel [111]$ or $[112]$. As the magnetic point group of E_2 -order is $-42m$, when $\mathbf{B} \parallel [001]$ ($[110]$), the system has C_{2z} ($\sigma_{[110]}$), so $\mathbf{M}_\perp = 0$. On the other hand, when $\mathbf{B} \parallel [111]$ or $[112]$, all symmetries are broken, so $\mathbf{M}_\perp \neq 0$.

3. $\text{Eu}_2\text{Ir}_2\text{O}_7$

$\text{Eu}_2\text{Ir}_2\text{O}_7$ is also a pyrochlore material, where only Ir electrons have magnetism. Because of crystal field and spin-orbital coupling, Ir^{4+} carry the effective spin $J = 1/2$. The ground state is known to be A_2 -octupole at low temperature. It is reported that when \mathbf{B} is applied in xy -plane the OM \mathbf{M}_O arises.²¹ $\mathbf{M}_O \propto B^2 \sin \theta \cos \theta \hat{z}$ is observed when the field-cooling direction is parallel to \hat{y} .

The OM can be compared with TM. When $\mathbf{B} \parallel \hat{x}$ or \hat{y} , $\mathbf{M}_\perp = 0$, according to Table S1 because of C_2 symmetry. Moreover, considering S_4T symmetry along z -direction, $\mathbf{M}_\perp \propto B^2 \sin(2\theta) \hat{z}$ which is consistent with \mathbf{M}_O result. We note that in the case of A_2 -octupole, \mathbf{M}_\perp and \mathbf{M}_O show the same B^2 and angular dependence. Thus, we cannot rule out the spin canting contribution to OM in the measured data.

Appendix G: The phenomenological model for anomalous and planar Hall Effect

The physical situation of planar Hall Effect is given in Fig. 4a of our manuscript. When we let $\hat{x} = [1\bar{1}0]$, $\hat{y} = [11\bar{2}]$, $\hat{z} = [111]$, the electric field is applied along \hat{x} , and the magnetic field is rotating within xy -plane ($\mathbf{B} = B(\cos \theta, \sin \theta, 0)$).

We can acquire a general form of TM by using symmetry analysis. We divide the component of TM into two, $\mathbf{M}_\perp = \mathbf{M}_{\perp, \text{in}} + \mathbf{M}_{\perp, \text{out}}$. Along $[111]$, C_3 rotation exists. Hence, both in-plane and out-of-plane components obey $a_0 + a_1 \cos 3\theta + a_2 \sin 3\theta$. During the rotation of magnetic field, the antiunitary mirror is present when $\theta = \pi/6 + n\pi/3$. The antiunitary is spanned by \hat{z} and \mathbf{B} , so that the TM can only arise along \hat{z} . Thus, the antiunitary mirror makes the in-plane TM vanishes. This gives the condition of TM components.

$$\begin{aligned}\mathbf{M}_{\perp, \text{out}} &= (A_0 + A_1 \cos 3\theta + A_2 \sin 3\theta) \hat{z}, \\ \mathbf{M}_{\perp, \text{in}} &= (B_1 \cos 3\theta) \hat{p},\end{aligned}\quad (\text{G1})$$

where $\hat{p} = (-\sin \theta, \cos \theta, 0)$ is the unit vector perpendicular to \mathbf{B} . The anomalous Hall conductivity is proportional to

$\mathbf{M}_{\perp, out}$, so

$$\sigma_{xy}^{AHE} \propto (A_0 + A_1 \cos 3\theta + A_2 \sin 3\theta). \quad (\text{G2})$$

For planar Hall Effect, we first address the Onsager's reciprocal relation. The Onsager's reciprocal relations state that the phenomenological tensors of a certain flow and force in a system out of equilibrium are symmetric. For example, the electrical conductivity under magnetic field \vec{H} and magnetization \vec{M} is given by

$$\sigma_{ij}(\vec{H}, \vec{M}) = \sigma_{ji}(-\vec{H}, -\vec{M}) \quad (\text{G3})$$

Upon this, we assume that the system has a cubic symmetry. By using these two constraints, the current density can be expanded up to the first order of electric field and the second

order of magnetic field and magnetization.^{38,45,46} That is,

$$\begin{aligned} \vec{J} = & \sigma_0 \vec{E} + \sigma_1 \vec{E} \times \vec{H} + \sigma_2 H^2 \vec{E} + \sigma_3 (\vec{E} \cdot \vec{H}) \vec{H} + \sigma_4 M^2 \vec{E} \\ & + \sigma_5 (\vec{E} \times \vec{M}) + \sigma_6 (\vec{E} \cdot \vec{M}) \vec{M} + \sigma_7 (\vec{M} \cdot \vec{H}) \vec{E} \\ & + \sigma_8 (\vec{M} \times (\vec{H} \times \vec{E}) + \vec{H} \times (\vec{M} \times \vec{E})) \end{aligned} \quad (\text{G4})$$

and the conductivity is

$$\begin{aligned} \sigma_{ij} = & (\sigma_0 + \sigma_2 H^2 + \sigma_4 M^2 + (\sigma_7 - 2\sigma_8)(\vec{M} \cdot \vec{H})) \delta_{ij} \\ & + \sigma_1 \epsilon_{ijk} H_k + \sigma_5 \epsilon_{ijk} M_k \\ & + \sigma_3 H_i H_j + \sigma_6 M_i M_j + \sigma_8 (M_i H_j + H_i M_j). \end{aligned} \quad (\text{G5})$$

The first line indicates the magnetoconductivity. The second line indicates the conventional and anomalous Hall conductivities. The last line gives the phenomenological form of PHC,

$$\begin{aligned} \sigma_{xy}^{PHE} = & \sigma_3 H_x H_y + \sigma_6 M_x M_y \\ & + \sigma_8 (M_x H_y + H_x M_y). \end{aligned} \quad (\text{G6})$$

This is the equation that we are based on. Let $\mathbf{M} = \mathbf{M}_{\perp, in}$ above, then the angular dependence of PHC is

$$\begin{aligned} \sigma_{xy}^{PHE} = & A_1 \cos \theta + A_2 \cos 5\theta \\ & + B_1 \sin 2\theta + B_2 \sin 4\theta + B_3 \sin 8\theta. \end{aligned} \quad (\text{G7})$$

* bjyang@snu.ac.kr

¹ Y. Tokura, K. Yasuda, and A. Tsukazaki, Magnetic topological insulators, *Nature Reviews Physics* **1**, 126 (2019).

² W. Witczak-Krempa, G. Chen, Y. B. Kim, and L. Balents, Correlated quantum phenomena in the strong spin-orbit regime, *Annual Review of Condensed Matter Physics* **5**, 57 (2014).

³ M.-T. Suzuki, T. Koretsune, M. Ochi, and R. Arita, Cluster multipole theory for anomalous Hall effect in antiferromagnets, *Physical Review B* **95**, 094406 (2017).

⁴ M.-T. Suzuki, T. Nomoto, R. Arita, Y. Yanagi, S. Hayami, and H. Kusunose, Multipole expansion for magnetic structures: A generation scheme for a symmetry-adapted orthonormal basis set in the crystallographic point group, *Physical Review B* **99**, 174407 (2019).

⁵ L. Šmejkal, R. González-Hernández, T. Jungwirth, and J. Sinova, Crystal time-reversal symmetry breaking and spontaneous Hall effect in collinear antiferromagnets, *Science advances* **6**, eaaz8809 (2020).

⁶ Y. Gao and D. Xiao, Orbital magnetic quadrupole moment and nonlinear anomalous thermoelectric transport, *Physical Review B* **98**, 060402 (2018).

⁷ R. Matsumoto, R. Shindou, and S. Murakami, Thermal hall effect of magnons in magnets with dipolar interaction, *Physical Review B* **89**, 054420 (2014).

⁸ E. Mishchenko and O. Starykh, Equilibrium currents in chiral systems with nonzero chern number, *Physical Review B* **90**, 035114 (2014).

⁹ V. A. Zyuzin and A. A. Kovalev, Magnon spin nernst effect in antiferromagnets, *Physical review letters* **117**, 217203 (2016).

¹⁰ R. Cheng, S. Okamoto, and D. Xiao, Spin nernst effect of

magnons in collinear antiferromagnets, *Physical review letters* **117**, 217202 (2016).

¹¹ S. Park, N. Nagaosa, and B.-J. Yang, Thermal Hall Effect, Spin Nernst Effect, and spin density induced by a thermal gradient in collinear ferrimagnets from magnon-phonon interaction, *Nano letters* **20**, 2741 (2020).

¹² W. J. Kim, J. H. Gruenewald, T. Oh, S. Cheon, B. Kim, O. B. Korneta, H. Cho, D. Lee, Y. Kim, M. Kim, et al., Unconventional anomalous Hall effect from antiferromagnetic domain walls of Nd₂Ir₂O₇ thin films, *Physical Review B* **98**, 125103 (2018).

¹³ K. Ueda, T. Oh, B.-J. Yang, R. Kaneko, J. Fujioka, N. Nagaosa, and Y. Tokura, Magnetic-field induced multiple topological phases in pyrochlore iridates with mott criticality, *Nature communications* **8**, 1 (2017).

¹⁴ K. Ueda, R. Kaneko, H. Ishizuka, J. Fujioka, N. Nagaosa, and Y. Tokura, Spontaneous Hall effect in the Weyl semimetal candidate of all-in all-out pyrochlore iridate, *Nature communications* **9**, 1 (2018).

¹⁵ T. Ohtsuki, Z. Tian, A. Endo, M. Halim, S. Katsumoto, Y. Kohama, K. Kindo, M. Lippmaa, and S. Nakatsuji, Strain-induced spontaneous Hall effect in an epitaxial thin film of a Luttinger semimetal, *PNAS* **116**, 8803 (2019).

¹⁶ Y. Zhang, J. Železný, Y. Sun, J. Van Den Brink, and B. Yan, Spin Hall effect emerging from a noncollinear magnetic lattice without spin-orbit coupling, *New Journal of Physics* **20**, 073028 (2018).

¹⁷ S. Abarzhi, A. Bazhan, L. Prozorova, and I. Zaliznyak, Spin reorientation in the easy-plane hexagonal antiferromagnet under a canted magnetic field, *Journal of Physics: Condensed Matter* **4**, 3307 (1992).

¹⁸ V. Glazkov, M. Zhitomirsky, A. Smirnov, H.-A. K. von Nidda,

- A. Loidl, C. Marin, and J.-P. Sanchez, Single-ion anisotropy in the gadolinium pyrochlores studied by electron paramagnetic resonance, *Physical Review B* **72**, 020409 (2005).
- ¹⁹ V. Glazkov, C. Marin, and J. Sanchez, Observation of a transverse magnetization in the ordered phases of the pyrochlore magnet $\text{Gd}_2\text{Ti}_2\text{O}_7$, *Journal of Physics: Condensed Matter* **18**, L429 (2006).
- ²⁰ V. Glazkov, M. Zhitomirsky, A. Smirnov, C. Marin, J. Sanchez, A. Forget, D. Colson, and P. Bonville, Single-ion anisotropy and transverse magnetization in the frustrated gadolinium pyrochlores, *Journal of Physics: Condensed Matter* **19**, 145271 (2007).
- ²¹ T. Liang, T. H. Hsieh, J. J. Ishikawa, S. Nakatsuji, L. Fu, and N. Ong, Orthogonal magnetization and symmetry breaking in pyrochlore iridate $\text{Eu}_2\text{Ir}_2\text{O}_7$, *Nature Physics* **13**, 599 (2017).
- ²² Y. Li, T. Oh, J. Son, J. Song, M. K. Kim, D. Song, S. Kim, S. H. Chang, C. Kim, B.-J. Yang, et al., Correlated magnetic weyl semimetal state in strained $\text{Pr}_2\text{Ir}_2\text{O}_7$, *Advanced Materials*, 2008528 (2021).
- ²³ R. Battilomo, N. Scopigno, and C. Ortix, Anomalous planar Hall effect in two-dimensional trigonal crystals, *Physical Review Research* **3**, L012006 (2021).
- ²⁴ T. Oh, H. Ishizuka, and B.-J. Yang, Magnetic field induced topological semimetals near the quantum critical point of pyrochlore iridates, *Physical Review B* **98**, 144409 (2018).
- ²⁵ W. J. Kim, T. Oh, J. Song, E. K. Ko, Y. Li, J. Mun, B. Kim, J. Son, Z. Yang, Y. Kohama, et al., Strain engineering of the magnetic multipole moments and anomalous hall effect in pyrochlore iridate thin films, *Science Advances* **6**, eabb1539 (2020).
- ²⁶ S. Palmer and J. Chalker, Order induced by dipolar interactions in a geometrically frustrated antiferromagnet, *Physical Review B* **62**, 488 (2000).
- ²⁷ M. Elhajal, B. Canals, R. Sunyer, and C. Lacroix, Ordering in the pyrochlore antiferromagnet due to dzyaloshinsky-moriya interactions, *Physical Review B* **71**, 094420 (2005).
- ²⁸ M. J. Gingras and P. A. McClarty, Quantum spin ice: a search for gapless quantum spin liquids in pyrochlore magnets, *Reports on Progress in Physics* **77**, 056501 (2014).
- ²⁹ Y. Zhang, Y. Sun, H. Yang, J. Železný, S. P. Parkin, C. Felser, and B. Yan, Strong anisotropic anomalous Hall effect and spin Hall effect in the chiral antiferromagnetic compounds Mn_3X ($\text{x} = \text{Ge, Sn, Ga, Ir, Rh, and Pt}$), *Physical Review B* **95**, 075128 (2017).
- ³⁰ I. Tomeno, H. N. Fuke, H. Iwasaki, M. Sahashi, and Y. Tsunoda, Magnetic neutron scattering study of ordered Mn_3Ir , *Journal of applied physics* **86**, 3853 (1999).
- ³¹ J. M. Taylor, E. Lesne, A. Markou, F. K. Dejene, B. Ernst, A. Kalache, K. G. Rana, N. Kumar, P. Werner, C. Felser, et al., Epitaxial growth, structural characterization, and exchange bias of noncollinear antiferromagnetic Mn_3Ir thin films, *Physical Review Materials* **3**, 074409 (2019).
- ³² H. Chen, Q. Niu, and A. H. MacDonald, Anomalous Hall effect arising from noncollinear antiferromagnetism, *Physical review letters* **112**, 017205 (2014).
- ³³ J. S. Gardner, M. J. Gingras, and J. E. Greedan, Magnetic pyrochlore oxides, *Reviews of Modern Physics* **82**, 53 (2010).
- ³⁴ R. Moessner and J. T. Chalker, Properties of a classical spin liquid: the heisenberg pyrochlore antiferromagnet, *Physical review letters* **80**, 2929 (1998).
- ³⁵ S. Nandy, G. Sharma, A. Taraphder, and S. Tewari, Chiral anomaly as the origin of the planar Hall effect in weyl semimetals, *Physical Review Letters* **119**, 176804 (2017).
- ³⁶ S.-H. Zheng, H.-J. Duan, J.-K. Wang, J.-Y. Li, M.-X. Deng, and R.-Q. Wang, Origin of planar Hall effect on the surface of topological insulators: Tilt of dirac cone by an in-plane magnetic field, *Physical Review B* **101**, 041408 (2020).
- ³⁷ V. Ky, Plane Hall effect in ferromagnetic metals, *Soviet Physics JETP* **23**, 809 (1966).
- ³⁸ Y. Wang, P. A. Lee, D. Silevitch, F. Gomez, S. Cooper, Y. Ren, J.-Q. Yan, D. Mandrus, T. Rosenbaum, and Y. Feng, Antisymmetric linear magnetoresistance and the planar Hall effect, *Nature Communications* **11**, 1 (2020).
- ³⁹ S. Nandy, A. Taraphder, and S. Tewari, Berry phase theory of planar Hall effect in topological insulators, *Scientific reports* **8**, 1 (2018).
- ⁴⁰ W. Witczak-Krempa, A. Go, and Y. B. Kim, Pyrochlore electrons under pressure, heat, and field: Shedding light on the iridates, *Physical Review B* **87**, 155101 (2013).
- ⁴¹ N. Nagaosa, J. Sinova, S. Onoda, A. H. MacDonald, and N. P. Ong, Anomalous Hall effect, *Reviews of modern physics* **82**, 1539 (2010).
- ⁴² G. Sim and S. Lee, Discovery of a new type of magnetic order on pyrochlore spinels, *Physical Review B* **98**, 014423 (2018).
- ⁴³ A. Chubukov, Quasi-one-dimensional hexagonal antiferromagnets in a magnetic field, *Journal of Physics C: Solid State Physics* **21**, L441 (1988).
- ⁴⁴ J. Stewart, G. Ehlers, A. Wills, S. T. Bramwell, and J. Gardner, Phase transitions, partial disorder and multi-k structures in $\text{Gd}_2\text{Ti}_2\text{O}_7$, *Journal of Physics: Condensed Matter* **16**, L321 (2004).
- ⁴⁵ F. Seitz, Note on the theory of resistance of a cubic semiconductor in a magnetic field, *Physical Review* **79**, 372 (1950).
- ⁴⁶ A. B. Pippard, *Magnetoresistance in metals*, Vol. 2 (Cambridge university press, 1989).